DRAFT VERSION JANUARY 17, 2016
Preprint typeset using LaTeX style emulateapj v. 12/16/11

arXiv:1301.1228v2 [astro-ph.CO] 20 Mar 2013

NEW CONSTRAINTS ON COSMIC REIONIZATION FROM THE 2012 HUBBLE ULTRA DEEP FIELD CAMPAIGN

BRANT E. ROBERTSON[1], STEVEN R. FURLANETTO[2], EVAN SCHNEIDER[1], STEPHANE CHARLOT[3], RICHARD S. ELLIS[4], DANIEL P. STARK[1], ROSS J. MCLURE[5], JAMES S. DUNLOP[5], ANTON KOEKEMOER[6], MATTHEW A. SCHENKER[4], MASAMI OUCHI[7], YOSHIAKI ONO[7], EMMA CURTIS-LAKE[5], ALEXANDER B. ROGERS[5], REBECCA A. A. BOWLER[5], MICHELE CIRASUOLO[5]

Draft version January 17, 2016

ABSTRACT

Understanding cosmic reionization requires the identification and characterization of early sources of hydrogen-ionizing photons. The 2012 Hubble Ultra Deep Field (UDF12) campaign has acquired the deepest infrared images with the Wide Field Camera 3 aboard *Hubble Space Telescope* and, for the first time, systematically explored the galaxy population deep into the era when cosmic microwave background (CMB) data indicates reionization was underway. The UDF12 campaign thus provides the best constraints to date on the abundance, luminosity distribution, and spectral properties of early star-forming galaxies. We synthesize the new UDF12 results with the most recent constraints from CMB observations to infer redshift-dependent ultraviolet (UV) luminosity densities, reionization histories, and electron scattering optical depth evolution consistent with the available data. Under reasonable assumptions about the escape fraction of hydrogen ionizing photons and the intergalactic medium clumping factor, we find that to fully reionize the universe by redshift $z \sim 6$ the population of star-forming galaxies at redshifts $z \sim 7-9$ likely must extend in luminosity below the UDF12 limits to absolute UV magnitudes of $M_{\rm UV} \sim -13$ or fainter. Moreover, low levels of star formation extending to redshifts $z \sim 15-25$, as suggested by the normal UV colors of $z \simeq$7-8 galaxies and the smooth decline in abundance with redshift observed by UDF12 to $z \simeq 10$, are additionally likely required to reproduce the optical depth to electron scattering inferred from CMB observations.

Subject headings: cosmology:reionization – galaxies:evolution – galaxies:formation

1. INTRODUCTION

The process of cosmic reionization remains one of the most important outstanding problems in galaxy formation and cosmology. After recombination at $z \approx 1090$ (Hinshaw et al. 2012), gas in the universe was mostly neutral. However, observations of the Gunn & Peterson (1965) trough in quasar spectra (e.g., Fan et al. 2001, 2002, 2003, 2006b; Djorgovski et al. 2001) indicate that intergalactic gas has become almost fully reionized by redshift $z \sim 5$. The electron scattering optical depth inferred from CMB observations suggests that if the universe was instantaneously reionized, then reionization would occur as early as redshift $z \approx 10$ (Spergel et al. 2003; Hinshaw et al. 2012). Given the dramatic decline in the abundance of quasars beyond redshift $z \sim 6$, they very likely cannot be a significant contributor to cosmic reionization (e.g., Willott et al. 2010; Fontanot et al. 2012) even though quasars have been discovered as early as $z \sim 7$ (Mortlock et al. 2011). Star-forming galaxies at redshifts $z \gtrsim 6$ have therefore long been postulated as the likely agents of cosmic reionization, and their time-dependent abundance and spectral properties are thus crucial ingredients for understanding how intergalactic hydrogen became reionized (for reviews, see Fan et al. 2006a; Robertson et al. 2010; Loeb & Furlanetto 2012).

We present an analysis of the implications of the 2012 Hubble Ultra Deep Field[8] (UDF12) campaign results on the abundance and spectral characteristics of galaxies at $z \sim 7-12$ for the reionization process. The UDF12 campaign is a 128-orbit *Hubble Space Telescope* (*HST*) program (GO 12498, PI: Ellis) with the infrared (IR) channel on the Wide Field Camera 3 (WFC3/IR) that acquired the deepest ever images in the IR with *HST* in the Hubble Ultra Deep Field (HUDF) in Fall 2012 (the UDF12 project and data overview are described in Ellis et al. 2013 and Koekemoer et al. 2013). Combined with previous HUDF observations (GO 11563, PI: G. Illingworth; GO 12060, 12061, 12062, PIs: S. Faber and H. Ferguson; GO 12099, PI: A. Riess), the UDF12 imaging reaches depths of $Y_{105} = 30$, $J_{125} = 29.5$, $J_{140} = 29.5$, and $H_{160} = 29.5$ ($5-\sigma$ AB magnitudes). The UDF12 observations have provided the first determinations of the galaxy abundance at redshifts $8.5 \leq z \leq 12$ (Ellis et al. 2013), precise determinations of the galaxy luminosity function at redshifts $z \sim 7-8$ (Schenker et al. 2012a; McLure et al. 2012), robust ultraviolet (UV) spectral slope measurements at $z \sim 7-8$ (Dunlop et al. 2012b), and size-luminosity relation measures at redshifts $z \sim 6-8$ (Ono et al. 2012a).

Our earlier UDF12 publications already provide some new constraints on the role that galaxies play in cosmic reionization and the duration of the process. In Ellis et al. (2013), we argued that continuity in the declining abundance of star-forming galaxies over $6 < z < 10$ (and possibly to $z \simeq 12$), implied the likelihood of further star formation beyond the redshift limits currently probed. Likewise, in Dunlop et al. (2012b), the constancy of the UV continuum slope measured in $z \simeq 7-9$ galaxies over a wide range in luminosity supports

[1] Department of Astronomy and Steward Observatory, University of Arizona, Tucson AZ 85721
[2] Department of Physics & Astronomy, University of California, Los Angeles CA 90095
[3] UPMC-CNRS, UMR7095, Institut d'Astrophysique de Paris, F-75014, Paris, France
[4] Department of Astrophysics, California Institute of Technology, MC 249-17, Pasadena, CA 91125
[5] Institute for Astronomy, University of Edinburgh, Royal Observatory, Edinburgh EH9 3HJ, UK
[6] Space Telescope Science Institute, Baltimore, MD 21218
[7] Institute for Cosmic Ray Research, University of Tokyo, Kashiwa City, Chiba 277-8582, Japan

[8] http://udf12.arizona.edu

the contention that the bulk of the stars at this epoch are already enriched by earlier generations. Collectively, these two results support an extended reionization process.

We synthesize these UDF12 findings with the recent 9-year *Wilkinson Microwave Anisotropy Probe* (*WMAP*) results (Hinshaw et al. 2012) and stellar mass density measurements (Stark et al. 2012) to provide new constraints on the role of high-redshift star-forming galaxies in the reionization process. Enabled by the new observational findings, we perform Bayesian inference using a simple parameterized model for the evolving UV luminosity density to find reionization histories, stellar mass density evolutions, and electron scatter optical depth progressions consistent with the available data. We limit the purview of this paper to empirical modeling of the reionization process, and comparisons with more detailed galaxy formation models will be presented in a companion paper (Dayal et al., in preparation).

Throughout this paper, we assume the 9-year *WMAP* cosmological parameters (as additionally constrained by external CMB datasets; $h = 0.705$, $\Omega_{\rm m} = 0.272$, $\Omega_\Lambda = 0.728$, $\Omega_{\rm b} = 0.04885$). Magnitudes are reported using the AB system (Oke & Gunn 1983). All Bayesian inference and maximum likelihood fitting is performed using the *MultiNest* code (Feroz & Hobson 2008; Feroz et al. 2009).

2. THE PROCESS OF COSMIC REIONIZATION

Theoretical models of the reionization process have a long history. Early analytic and numerical models of the reionization process (e.g., Madau et al. 1999; Miralda-Escudé et al. 2000; Gnedin 2000; Barkana & Loeb 2001; Razoumov et al. 2002; Wyithe & Loeb 2003; Ciardi et al. 2003) highlighted the essential physics that give rise to the ionized intergalactic medium (IGM) at late times. In the following description of the cosmic reionization process we follow most closely the modeling of Madau et al. (1999), Bolton & Haehnelt (2007b), Robertson et al. (2010), and Kuhlen & Faucher-Giguère (2012), but there has been closely related recent work by Ciardi et al. (2012) and Jensen et al. (2013).

The reionization process is a balance between the recombination of free electrons with protons to form neutral hydrogen and the ionization of hydrogen atoms by cosmic Lyman continuum photons with energies $E > 13.6$ eV. The dimensionless volume filling fraction of ionized hydrogen $Q_{\rm HII}$ can be expressed as a time-dependent differential equation capturing these competing effects as

$$\dot{Q}_{\rm HII} = \frac{\dot{n}_{\rm ion}}{\langle n_{\rm H}\rangle} - \frac{Q_{\rm HII}}{t_{\rm rec}} \tag{1}$$

where dotted quantities are time derivatives.

The comoving density of hydrogen atoms

$$\langle n_{\rm H}\rangle = X_{\rm p}\Omega_{\rm b}\rho_{\rm c} \tag{2}$$

depends on the primordial mass-fraction of hydrogen $X_{\rm p} = 0.75$ (e.g., Hou et al. 2011), the critical density $\rho_{\rm c} = 1.8787 \times 10^{-29} h^{-2}$ g cm^3, and the fractional baryon density $\Omega_{\rm b}$.

As a function of redshift, the average recombination time in the IGM is

$$t_{\rm rec} = \left[C_{\rm HII}\alpha_{\rm B}(T)(1+Y_{\rm p}/4X_{\rm p})\langle n_{\rm H}\rangle(1+z)^3\right]^{-1}, \tag{3}$$

where $\alpha_{\rm B}(T)$ is the case B recombination coefficient for hydrogen (we assume an IGM temperature of $T = 20,000$K), $Y_{\rm p} = 1 - X_{\rm p}$ is the primordial helium abundance (and accounts for the number of free electrons per proton in the fully ionized IGM, e.g., Kuhlen & Faucher-Giguère 2012), and $C_{\rm HII} \equiv \langle n_{\rm H}^2\rangle/\langle n_{\rm H}\rangle^2$ is the "clumping factor" that accounts for the effects of IGM inhomogeneity through the quadratic dependence of the recombination rate on density.

Simulations suggest that the clumping factor of IGM gas is $C_{\rm HII} \approx 1-6$ at the redshifts of interest (e.g., Sokasian et al. 2003; Iliev et al. 2006; Pawlik et al. 2009; Shull et al. 2012; Finlator et al. 2012). While early hydrodynamical simulation studies suggested that the clumping factor could be as high as $C_{\rm HII} \sim 10-40$ at redshifts $z < 8$ (e.g., Gnedin & Ostriker 1997), recent studies that separately identify IGM and interstellar medium gas in the simulations and employ a more detailed modeling of the evolving UV background have found lower values of $C_{\rm HII}$. An interesting study of the redshift evolution of the clumping factor was provided by Pawlik et al. (2009, see their Figures 5 and 7). At early times in their simulations ($z \geq 10$), the clumping factor was low ($C_{\rm HII} < 3$) but increased with decreasing redshift at a rate similar to predictions from the Miralda-Escudé et al. (2000) model of the evolving IGM density probability distribution function. In the absence of photoheating, at lower redshifts ($z \lesssim 9$) the clumping factor would begin to increase more rapidly than the Miralda-Escudé et al. (2000) prediction to reach $C_{\rm HII} \sim 10-20$ by $z \sim 6$. In the presence of photoheating, the evolution of the clumping factor depends on the epoch when the uniform UV background becomes established. If the IGM was reheated early ($z \sim 10-20$) the predicted rise in clumping factor breaks after the UV background is established and increases only slowly to $C_{\rm HII} \sim 3-6$ at late times ($z \sim 6$). If instead, and perhaps more likely, the IGM is reheated later (e.g, $z \sim 6-8$) the clumping factor may actually decrease at late times from $C_{\rm HII} \sim 6-10$ at $z \sim 8$ to $C_{\rm HII} \sim 3-6$ at $z \sim 6$.

The results of these simulations (e.g., Pawlik et al. 2009; Finlator et al. 2012) in part motivate our choice to treat the clumping factor as a constant $C_{\rm HII} \sim 3$ since over a wide range of possible redshifts for the establishment of the UV background the clumping factor is expected to be $C_{\rm HII} \sim 2-4$ at $z \lesssim 12$ (see Figure 5 of Pawlik et al. 2009) and lower at earlier times. In comparison with our previous work (Robertson et al. 2010), where we considered $C_{\rm HII} = 2-6$ and frequently used $C_{\rm HII} = 2$ in Equation 3, we will see that our models complete reionization somewhat later when a somewhat larger value of $C_{\rm HII}$ is more appropriate. However, we note that the end of the reionization process may be more complicated than what we have described above (see, e.g., Section 9.2.1 of Loeb & Furlanetto 2012). As reionization progresses, the ionized phase penetrates more and more deeply into dense clumps within the IGM – the material that will later form the Lyman-α forest (and higher column density systems). These high-density clumps recombine much faster than average, so $C_{\rm HII}$ may increase throughout reionization (Furlanetto & Oh 2005). Combined with the failure of Equation 1 to model the detailed distribution of gas densities in the IGM, we expect our admittedly crude approach to fail at the tail end of reionization. Fortunately, we are primarily concerned with the middle phases of reionization here, so any unphysical behavior when $Q_{\rm HII}$ is large is not important for us.

The comoving production rate $\dot{n}_{\rm ion}$ of hydrogen-ionizing photons available to reionize the IGM depends on the intrinsic productivity of Lyman continuum radiation by stellar populations within galaxies parameterized in terms of the rate of

hydrogen-ionizing photons per unit UV (1500Å) luminosity $\xi_{\rm ion}$ (with units of ergs^{-1} Hz), the fraction $f_{\rm esc}$ of such photons that escape to affect the IGM, and the total UV luminosity density $\rho_{\rm UV}$ (with units of ergs s^{-1} Hz^{-1} Mpc^{-3}) supplied by star-forming galaxies to some limiting absolute UV magnitude $M_{\rm UV}$. The product

$$\dot{n}_{\rm ion} = f_{\rm esc}\xi_{\rm ion}\rho_{\rm UV} \quad (4)$$

then determines the newly available number density of Lyman continuum photons per second capable of reionizing intergalactic hydrogen. We note that the expression of $\dot{n}_{\rm ion}$ in terms of UV luminosity density rather than star formation rate (c.f., Robertson et al. 2010) is largely a matter of choice; stellar population synthesis models with assumed star formation histories are required to estimate $\xi_{\rm ion}$ and using the star formation rate density $\rho_{\rm SFR}$ in Equation 4 therefore requires no additional assumptions. Throughout this paper, we choose $f_{\rm esc} = 0.2$. As shown by Ouchi et al. (2009), escape fractions comparable to or larger than $f_{\rm esc} = 0.2$ during the reionization epoch are required for galaxies with typical stellar populations to contribute significantly. We also consider an evolving $f_{\rm esc}$ with redshift, with the results discussed in Section 6.2 below.

The advances presented in this paper come primarily from the new UDF12 constraints on the abundance of star-forming galaxies over $6.5 < z < 12$, the luminosity functions down to $M_{\rm UV} \simeq -17$, and robust determinations of their UV continuum colors. For the latter, in Section 3, we use the UV spectral slope of high-redshift galaxies by Dunlop et al. (2012b) and the stellar population synthesis models of Bruzual & Charlot (2003) to inform a choice for the number $\xi_{\rm ion}$ of ionizing photons produced per unit luminosity. For the former, the abundance and luminosity distribution of high-redshift galaxies determined by Ellis et al. (2013), Schenker et al. (2012a), and McLure et al. (2012) provide estimates of the evolving UV luminosity density $\rho_{\rm UV}$. The evolving UV luminosity density supplied by star-forming galaxies brighter than some limiting magnitude $M_{\rm UV}$ is simply related to an integral of the luminosity function as

$$\rho_{\rm UV}(z) = \int_{-\infty}^{M_{\rm UV}} \Phi(M)L(M)dM, \quad (5)$$

where L is the luminosity and the functional form of the galaxy luminosity function is often assumed to be a Schechter (1976) function

$$\Phi(M) = 0.4\ln 10\ \phi_\star \left[10^{0.4(M_\star - M)}\right]^{1+\alpha} \exp\left[-10^{0.4(M_\star - M)}\right] \quad (6)$$

parameterized in terms of the normalization $\phi_\star$ (in units of Mpc^{-3} mag^{-1}), the characteristic galaxy magnitude $M_\star$, and the faint-end slope α. Each of these parameters may evolve with redshift z, which can affect the relative importance of faint galaxies for reionization (e.g., Oesch et al. 2009; Bouwens et al. 2012b). In Sections 4 and 4.1 below, we present our method of using the previous and UDF12 data sets to infer constraints on the luminosity density as a function of redshift and limiting magnitude.

2.1. *Stellar Mass Density as a Constraint on Reionization*

The UV luminosity density is supplied by short-lived, massive stars and therefore reflects the time rate of change of the stellar mass density $\rho_\star(z)$. In the context of our model, there are two routes for estimating the stellar mass density. First, we can integrate the stellar mass density supplied by the star formation rate inferred from the evolving UV luminosity density as

$$\rho_\star(z) = (1-R)\int_{\infty}^{z} \eta_{\rm sfr}(z')\rho_{\rm UV}(z')\frac{dt}{dz'}dz', \quad (7)$$

where $\eta_{\rm sfr}(z)$ provides the stellar population model-dependent conversion between UV luminosity and star formation rate (in units $M_\odot$ yr^{-1} ergs^{-1} s Hz), R is the fraction of mass returned from a stellar population to the ISM (28% for a Salpeter 1955 model after ~ 10 Gyr for a $0.1-100M_\odot$ IMF), and dt/dz gives the rate of change of universal time per unit redshift (in units of yr). While $\eta_{\rm sfr}(z)$ is in principle time-dependent, there is no firm evidence yet of its evolution and we adopt a constant value throughout.

While the evolving stellar mass density can be calculated in our model, the observational constraints on $\rho_\star$ have involved integrating a composite stellar mass function constructed from the UV luminosity function and a stellar mass to UV luminosity relation (González et al. 2011; Stark et al. 2012, see also Labbe et al. 2012). Using near-IR observations with the *Spitzer Space Telescope*, stellar masses of UV-selected galaxies are measured as a function of luminosity. Stark et al. (2012) find that the stellar mass – $L_{\rm UV}$ relation, corrected for nebular emission contamination, is well described by

$$\log m_\star = 1.433\log L_{\rm UV} - 31.99 + f_\star(z) \quad (8)$$

where $m_\star$ is the stellar mass in $M_\odot$, $L_{\rm UV}$ is the UV luminosity density in ergs s^{-1} Hz^{-1}, and $f_\star(z) = [0, -0.03, -0.18, -0.40]$ for redshift $z \approx [4, 5, 6, 7]$.

The stellar mass density will then involve an integral over the product of the UV luminosity function and the stellar mass $m_\star(L_{\rm UV})$. However, the significant scatter in the $m_\star(L_{\rm UV})$ relation ($\sigma \approx 0.5$ in $\log m_\star$, see González et al. 2011; Stark et al. 2012) must be taken into account. The gaussian scatter $p[M' - M(\log m_\star)]$ in luminosity contributing at a given $\log m_\star$ can be incorporated into the stellar mass function $dn_\star/d\log m_\star$ with a convolution over the UV luminosity function. We write the stellar mass function as

$$\frac{dn_\star}{d\log m_\star} = \frac{dM}{d\log m_\star}\int_{-\infty}^{\infty} \Phi(M')p[M' - M(\log m_\star)]dM'. \quad (9)$$

For vanishing scatter Equation 9 would give simply $dn_\star/dm_\star = \Phi[M(m_\star)] \times dM/dm_\star$. The stellar mass density $\rho_\star$ can be computed by integrating this mass function as

$$\rho_\star(< m_\star, z) = \int_{-\infty}^{\log m_\star} \frac{dn_\star}{d\log m'_\star} m'_\star d\log m'_\star. \quad (10)$$

A primary feature of the stellar mass function is that the stellar mass – UV luminosity relation and scatter flattens it relative to the UV luminosity function. Correspondingly, the stellar mass density converges faster with decreasing stellar mass or luminosity than does the UV luminosity density (Equation 5). The stellar mass density then serves as an additional, integral constraint on $\dot{n}_{\rm ion}$.

2.2. *Electron Scattering Optical Depth*

Once the evolving production rate of ionizing photons $\dot{n}_{\rm ion}$ is determined, the reionization history $Q_{\rm HII}(z)$ of the universe can be calculated by integrating Equation 1. An important integral constraint on the reionization history is the electron scattering optical depth τ inferred from observations of the

CMB. The optical depth can be calculated from the reionization history as a function of redshift z as

$$\tau(z) = \int_0^z c\langle n_{\rm H}\rangle \sigma_{\rm T} f_{\rm e} Q_{\rm HII}(z') H(z')(1+z')^2 dz', \qquad (11)$$

where c is the speed of light, $\sigma_{\rm T}$ is the Thomson cross section, and $H(z)$ is the redshift-dependent Hubble parameter. The number $f_{\rm e}$ of free electrons per hydrogen nucleus in the ionized IGM depends on the ionization state of helium. Following Kuhlen & Faucher-Giguère (2012) and other earlier works, we assume that helium is doubly ionized ($f_{\rm e} = 1+Y_{\rm p}/2X_{\rm p}$) at $z \leq 4$ and singly ionized ($f_{\rm e} = 1+Y_{\rm p}/4X_{\rm p}$) at higher redshifts. To utilize the observational constraints on τ as a constraint on the reionization history, we employ the posterior probability distribution $p(\tau)$ determined from the Monte Carlo Markov Chains used in the 9-year *WMAP* results[9] as a marginalized likelihood for our derived τ values. This method is described in more detail in Section 5.

3. UV SPECTRAL SLOPES AND THE IONIZING PHOTON BUDGET

A critical ingredient for determining the comoving production rate of hydrogen ionizing photons is the ratio $\xi_{\rm ion}$ of the Lyman continuum photon emission rate per unit UV (1500Å) luminosity spectral density of individual sources. Since Lyman continuum photons are predominately produced by hot, massive, UV-bright stars, it is sensible to expect that $\xi_{\rm ion}$ will be connected with the UV spectral slope of a stellar population. Here, we use observational constraints on the UV slope of high-redshift galaxies determined from the UDF12 campaign by Dunlop et al. (2012b) and stellar population synthesis models by Bruzual & Charlot (2003, BC03) to estimate a physically-motivated $\xi_{\rm ion}$ consistent with the data. In this paper, we concentrate on placing constraints on $\xi_{\rm ion}$; for a much more detailed analysis and interpretation of the UV slope results from UDF12, please see Dunlop et al. (2012b).

Prior to the UDF12 program, observations of high-redshift galaxies in the HUDF09 WFC3/IR campaign provided a first estimate of the UV spectral slopes (β, where $f_\lambda \propto \lambda^\beta$) of $z \gtrsim 7$ galaxies. Early results from the HUDF09 team indicated that these high-redshift galaxies had extraordinarily blue UV slopes of $\beta \approx -3$ (Bouwens et al. 2010), much bluer than well-studied starburst galaxies at lower redshifts (e.g., Meurer et al. 1999). In the intervening period before the UDF12 data was acquired, several workers argued against such extreme values (Finkelstein et al. 2010, 2012; McLure et al. 2011; Dunlop et al. 2012a; Bouwens et al. 2012a; Rogers et al. 2012). The UDF12 campaign provided significantly deeper H_{160} imaging data used in the spectral slope determination (e.g., $\beta = 4.43(J_{125}-H_{160})-2$) at redshifts $z \sim 7-8$) and added J_{140} imaging that reduces potential observational biases and enables a first UV slope determination at $z \sim 9$. These measurements were presented by Dunlop et al. (2012b), whose results are discussed in the context of the present paper in Figure 1 (data points, left panel). Dunlop et al. (2012b) measured the spectral slope β as a function of galaxy luminosity and redshift in the range $-19.5 \leq M_{\rm UV} \leq -17.5$ at $z \sim 7-8$. Using their reported measurements (see their Table 1), we performed simple fits of a constant to their β values at each redshift separately and found maximum likelihood values of $\beta(z \sim 7) = -1.915$ and $\beta(z \sim 8) = -1.970$ (Figure 1, red lines in left panel) consistent with the single $M_{\rm UV} = -18$ $z \sim 9$ measurement of $\beta(z \sim 9) = -1.80 \pm 0.63$. The 68% credibility intervals on a constant β at each redshift (Figure 1, grey areas in left panel) suggest that across redshifts $z \sim 7-9$ galaxies are consistent with a non-evolving UV spectral slope in the range $-2.1 \leq \beta \leq -1.7$. The apparent constancy of β with redshift avoids the need for strong assumptions about the redshift evolution of galaxy properties.

To connect these UV spectral slope determinations to a value of $\xi_{\rm ion}$, we must rely on stellar population synthesis models. We use the standard BC03 models to extract model spectral of stellar populations with a range of star formation histories (bursts and constant star formation rates), metallicities ($Z = 0.0001-0.05$), dust absorption ($A_{\rm V} \approx 0.1-1$; calculated using the Charlot & Fall 2000 dust model) and initial mass functions (IMF; Chabrier 2003 and Salpeter 1955). These models provide both the Lyman continuum produced by hot stars and the full spectral energy distributions (SEDs) of the composite stellar population per unit star formation rate (SFR) or stellar mass. We determine $\xi_{\rm ion}$ for each model by dividing the Lyman continuum photon production rate per unit SFR or stellar mass by a 1500Å luminosity spectral density (in ergs s^{-1} Hz^{-1}) per unit SFR or stellar mass measured with a synthetic filter with a flat response and 100Å width. The model SFR or stellar mass then scales out of the ratio $\xi_{\rm ion}$ (with units ergs^{-1} Hz). By measuring the UV slope values of each model using synthetic photometry with the J_{125} and H_{160} total throughput response on SEDs redshifted appropriately for $z \sim 7$ observations, the value of $\xi_{\rm ion}$ for each model β can be studied as a function of age, metallicity, IMF, and star formation history. We have checked that our methods for measuring β and IR colors from the synthetic model spectra reproduce results from the literature (see Robertson et al. 2007 and Figure 2 of Rogers et al. 2012).

The right panel of Figure 1 shows the $\xi_{\rm ion}$ of a variety of BC03 constant SFR models as a function of UV slope β, over the range $-2.1 \lesssim \beta \lesssim -1.7$ suggested by the Dunlop et al. (2012b) color measurements and further constrained such that the age of the stellar populations is less than the age of the universe at redshift $z \sim 7$ ($t \approx 7.8 \times 10^8$ yr). We will limit our further discussion of BC03 models to constant SFR histories, as we find single bursts populations display too wide a range of $\xi_{\rm ion}$ with β to be tightly constrained by β alone (although limits on the luminosity will constrain the available $\xi_{\rm ion}$ for a given β for single burst models, without the individual SED fits to objects we cannot usefully constrain such models over the wide range of luminosity and redshifts we examine).

Three broad types of BC03 constant SFR models are consistent with values of $\beta = -2$. Generically, the BC03 constant SFR models evolve from large values of $\xi_{\rm ion}$ and large negative values of β at early times to a roughly horizontal evolution with constant $\xi_{\rm ion}$ with β increasing at late times ($t \gtrsim 10^8$ yr). Metal poor ($Z < Z_\odot$) constant SFR populations without dust produce values of β significantly bluer (more negative) than observed at $z \sim 7-9$ (Dunlop et al. 2012b). Mature ($\gtrsim 10^8$ yr old), metal-rich ($Z \sim Z_\odot$), dust free stellar populations evolve to a constant value of $\log \xi_{\rm ion} \approx 24.95-25.2$ log ergs^{-1} Hz over the observed β values (as Figure 1 indicates, the results are largely independent of IMF for constant SFR models). Applying a dust absorption of $A_{\rm V} \sim 0.1$ using the model of Charlot & Fall (2000, with parameters $\tau_{\rm V} = 0.25$ and an ISM attenuation fraction of 0.3) shifts the SED evolution tracks down in $\xi_{\rm ion}$ (from dust absorption) and to redder β, such that young, metal-rich stellar populations

[9] http://lambda.gsfc.nasa.gov

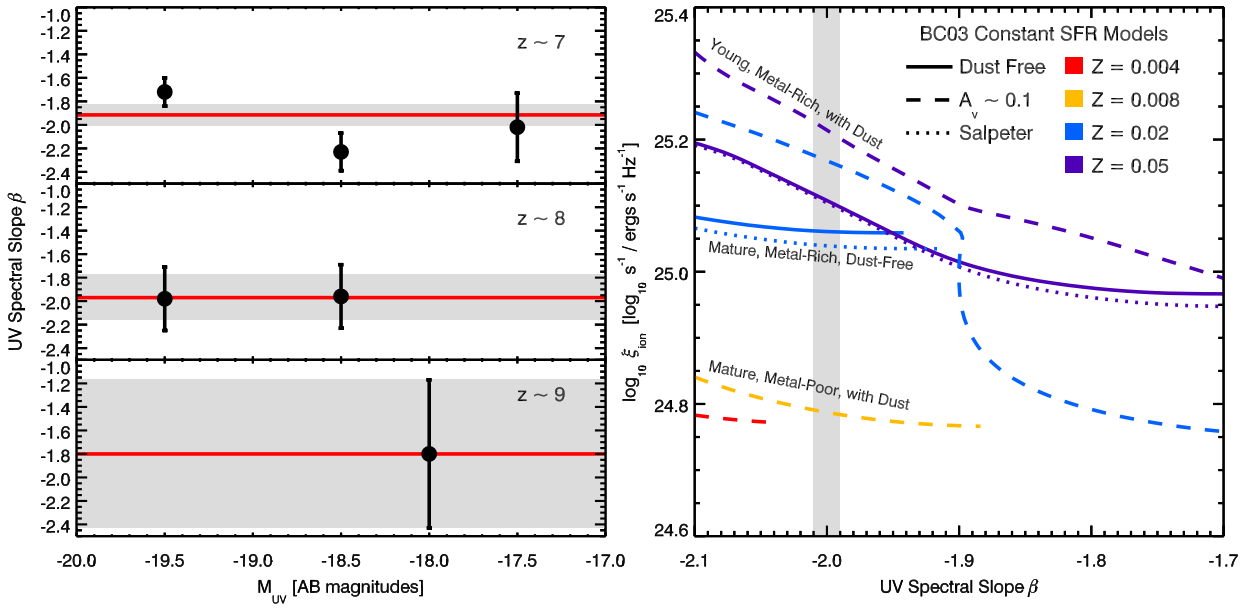

FIG. 1.— Spectral properties of high-redshift galaxies and the corresponding properties of stellar populations. Dunlop et al. (2012b) used the new UDF12 *HST* observations to measure the UV spectral slope β of $z \sim 7-9$ galaxies as a function of luminosity (data points, left panel). As the data are consistent with a constant β independent of luminosity, we have fit constant values of β at redshifts $z \sim 7-8$ (maximum likelihood values of $\beta(z \sim 7) = -1.915$ and $\beta(z \sim 8) = -1.970$ shown as red lines, inner 68% credibility intervals shown as grey shaded regions; at $z \sim 9$ the line and shaded region reflect the best fit value of $\beta(z \sim 9) = -1.80 \pm 0.63$). The data are broadly consistent with $\beta = -2$ (indicated with grey band in right panel), independent of redshift and luminosity. To translate the UV spectral slope to a ratio $\xi_{\rm ion}$ of ionizing photon production rate to UV luminosity, we use the Bruzual & Charlot (2003, BC03) stellar population synthesis models (right panel) assuming a constant star formation rate (SFR). The constant SFR models evolve from a declining $\xi_{\rm ion}$ with increasing β at early times to a relatively flat $\xi_{\rm ion}$ at late times (we plot the values of $\xi_{\rm ion}$ vs. β for population ages less than the age of the universe at $z \sim 7$, $t = 7.8 \times 10^8$ yr). Three broad types of BC03 constant SFR models are consistent with values of $\beta = -2$: mature ($\gtrsim 10^8$ yr old), metal-rich, dust free stellar populations, mature, metal-rich stellar populations with dust ($A_{\rm V} \sim 0.1$ calculated using the Charlot & Fall (2000) model), and young, metal-rich stellar populations with dust. Dust free models are plotted with solid lines, while dusty models are shown as dashed lines. We assume the Chabrier (2003) initial mass function (IMF), but the Salpeter (1955) IMF produces similar values of $\xi_{\rm ion}$ (dotted lines, dust-free case shown). Based on these models we optimistically assume $\log \xi_{\rm ion} = 25.2$ log ergs^{-1} Hz, but this value is conservative compared with assumptions widely used in the literature.

with dust can also reproduce values of $\beta \approx -2$ while maintaining $\log \xi_{\rm ion} = 24.75 - 25.35$ log ergs^{-1} Hz. Moderately metal-poor models ($Z \sim 0.2 - 0.4 Z_\odot$) with as much as $A_{\rm V} \approx 0.1$ can also reproduce $\beta \approx -2$ for population ages $t > 10^8$ yr, but the most metal poor models in this range require $t > 4 \times 10^8$ yr (an initial formation redshift of $z \gtrsim 12$ if observed at $z \sim 7$). We note that our conclusions about the connection between β (or $J_{125} - H_{160}$ color) and the properties of stellar populations is wholly consistent with previous results in the literature (e.g., Figure 7 of Finkelstein et al. 2010).

While the β measurements of Dunlop et al. (2012b) have greatly reduced the available BC03 stellar population model parameter space, there is still a broad allowable range of log $\xi_{\rm ion} \approx 24.75 - 25.35$ log ergs^{-1} Hz available for constant SFR models with UV spectral slopes of $\beta \approx -2$. We therefore adopt the value

$$\log \xi_{\rm ion} = 25.2 \ \log \ {\rm ergs}^{-1} \ {\rm Hz} \ \ ({\rm adopted}) \qquad (12)$$

throughout the rest of the paper. This $\xi_{\rm ion}$ is in the upper range of the available values shown in Figure 1, but is comparable to values adopted elsewhere in the literature (e.g., Kuhlen & Faucher-Giguère 2012, who assume $\log \xi_{\rm ion} \approx 25.3$ for $\beta = -2$, see their Equations 5 and 6).

We also considered stellar populations reddened by nebular continuum emission (e.g., Schaerer & de Barros 2009, 2010; Ono et al. 2010; Robertson et al. 2010), which in principle could allow relatively young, metal poor populations with larger $\xi_{\rm ion}$ to fall into the window of β values found by Dunlop et al. (2012b). We find that for $f_{\rm esc} \sim 0.2$, nebular models applied to young (< 100 Myr) constant star formation rate BC03 models are still marginally too blue ($\beta \sim -2.3$). Although more detailed modeling is always possible to explore the impact of nebular emission on $\xi_{\rm ion}$, the uniformity observed by Dunlop et al. (2012b) in the average value of β over a range in galaxy luminosities may argue against a diverse mixture young and mature stellar populations in the current $z \simeq 7-8$ samples. However, as Dunlop et al. (2012b) noted, a larger intrinsic scatter could be present in the UV slope distribution of the observed population but not yet detected. Similarly, top heavy initial mass function stellar populations with low metallicity, like the $1-100 M_\odot$ Salpeter IMF models of Schaerer (2003) used by Bouwens et al. (2010) to explain the earlier HUDF09 data, are disfavored owing to their blue spectral slopes.

For reference, for conversion from UV luminosity spectral density to SFR we note that for population ages $t > 10^8$ yr a constant SFR BC03 model with a Chabrier (2003) IMF and solar metallicity provides a 1500Å luminosity spectral density of

$$L_{\rm UV} \approx 1.25 \times 10^{28} \times \frac{\rm SFR}{M_\odot \ {\rm yr}^{-1}} \ {\rm ergs \ s^{-1} \ Hz^{-1}}, \qquad (13)$$

while, as noted by Madau et al. (1998), a comparable Salpeter (1955) model provides 64% of this UV luminosity. A very metal-poor population ($Z = Z_\odot/200$) would provide 40% more UV luminosity per unit SFR.

4. ULTRAVIOLET LUMINOSITY DENSITY

In addition to constraints on the spectral energy distributions of high-redshift galaxies (Dunlop et al. 2012b), the UDF12 observations provide a critical determination of the luminosity function of star forming galaxies at redshifts $7 \lesssim z \lesssim 9$. As described in Section 2, when calculating the comoving production rate $\dot{n}_{\rm ion}$ of hydrogen ionizing photons per unit volume (Equation 4) the UV luminosity density $\rho_{\rm UV}$ provided by an integral of the galaxy luminosity function is required (Equation 5). An accurate estimate of the $\rho_{\rm UV}$ provided by galaxies down to observed limits requires a careful analysis of star-forming galaxy samples at faint magnitudes. Using the UDF12 data, Schenker et al. (2012a) and McLure et al. (2012) have produced separate estimates of the $z \sim 7-8$ galaxy luminosity function for different sample selections (color-selected drop-out and spectral energy distribution-fitted samples, respectively). As we demonstrate, the UV luminosity densities computed from these separate luminosity functions are consistent within $1-\sigma$ at $z \sim 7$ and in even closer agreement at $z \sim 8$. Further, McLure et al. (2012) have provided the first luminosity function estimates at $z \sim 9$. Combined, these star-forming galaxy luminosity function determination provide the required constraints on $\rho_{\rm UV}$ in the epoch $z \gtrsim 7$ when, as we show below, the ionization fraction of the IGM is likely changing rapidly.

Given the challenge of working at the limits of the observational capabilities of *HST* and the relatively small volumes probed by the UDF (with expected cosmic variance of $\sim 30\%-40\%$ at redshifts $z \sim 7-9$, see Robertson 2010b,a; Muñoz et al. 2010, and Section 4.2.3 of Schenker et al. 2012a), we anchor our constraints on the evolving UV luminosity density with precision determinations of the galaxy luminosity function at redshifts $4 \lesssim z \lesssim 6$ by Bouwens et al. (2007).

To utilize as much information as possible about the luminosity function (LF) constraints at $z \sim 4-9$, we perform Bayesian inference to generate full posterior distributions of the galaxy luminosity functions at each redshift. To achieve this, we perform Schechter (1976) function parameter estimation at $z \sim 4-9$ using the stepwise maximum likelihood UV luminosity function constraints reported in Table 5 of Bouwens et al. (2007, for $z \sim 4-6$) and Table 2 of McLure et al. (2012, for $z \sim 7-8$) allowing all parameters (the luminosity function normalization $\phi_\star$, the characteristic galaxy magnitude $M_\star$, and the faint-end slope α) to vary. For these LF determinations, we assume Gaussian errors and a χ^2 likelihood. For additional constraints at $z \sim 7-8$, we use the samples from the full posterior distributions of LF parameters determined by Schenker et al. (2012a), using their method for Bayesian inference of LF parameters discussed in their Section 4.2. Lastly, at redshift $z \sim 9$ we perform parameter estimation on $\phi_\star$ given the stepwise maximum likelihood LF determination provided in Table 4 of McLure et al. (2012) while keeping $M_\star$ and α fixed at the best-fit $z \sim 8$ values reported by McLure et al. (2012). Again we assume Gaussian errors and a χ^2 likelihood. The limited information available at $z \sim 9$ and our restricted fitting method at this redshift mean that the inferred allowed variation in the $\rho_{\rm UV}(z \sim 9)$ will be underestimated. However, we have checked that this restriction does not strongly influence our results presented in Section 5. In each case our maximum likelihood luminosity function parameters are consistent within $1-\sigma$ of the values originally reported by Bouwens et al. (2007) and McLure et al. (2012), and are of course identical in the case of the Schenker et al. (2012a) LFs.

Figure 2 shows the integrated UV luminosity density $\rho_{\rm UV}$ as a function of limiting magnitude for these galaxy luminosity function determinations at $z \sim 5-8$ (constraints at $z \sim 4$ and $z \sim 9$ are also used). For each redshift, we show the maximum likelihood $\rho_{\rm UV}$ (white lines) and the inner 68% variation in the marginalized $\rho_{\rm UV}$ (blue regions). Since the luminosity functions are steep ($\alpha \lesssim -1.7$), the luminosity densities $\rho_{\rm UV}$ increase dramatically below the characteristic magnitude $M_\star$ at each redshift, but especially at $z \gtrsim 7$. The total $\rho_{\rm UV}$ supplied by star-forming galaxies therefore strongly depends on the limiting magnitude adopted to limit the integral in Equation 5. The UDF12 campaign depth of $M_{\rm UV} < -17$ provides $\rho_{\rm UV} \approx 10^{26}$ergs s^{-1} Hz^{-1} Mpc^{-3} at $z \sim 7$, declining to $\rho_{\rm UV} \sim 3.2 \times 10^{25}$ ergs s^{-1} Hz^{-1} Mpc^{-3} at $z \sim 8$. To put these $\rho_{\rm UV}$ values in context, we also indicate the critical values of $\rho_{\rm UV}$ required to keep $\dot{Q}_{\rm HII} = 0$ in Equation 1 and maintain reionization (grey areas and dashed line; assuming case A recombination[10]) if $f_{\rm esc} = 0.2$, $\log \xi_{\rm ion} = 25.2$ log ergs^{-1} Hz, and $C_{\rm HII} = 3$. Under these reasonable assumptions, the currently observed galaxy population clearly is not abundant enough to maintain reionization at $z \gtrsim 7$. Understanding the role of galaxies in the reionization process will therefore likely require extrapolations to luminosities beyond even the UDF12 depth, and the constraints on the LF shape achieved by the UDF12 observations will be important for performing these extrapolations reliably. The extent of the extrapolation down the luminosity function required for matching the reionization constraints depends in detail on our assumptions for the escape fraction $f_{\rm esc}$ or the ionizing photon production rate per UV luminosity $\xi_{\rm ion}$ of galaxies. We emphasize that the critical ionizing photon production rate $\dot{n}_{\rm ion}$ depends on the product $\dot{n}_{\rm ion} = f_{\rm esc}\xi_{\rm ion}\rho_{\rm UV}$, and will shift up or down proportionally to $f_{\rm esc}\xi_{\rm ion}$ at fixed $\rho_{\rm UV}$. Similarly, the $\dot{n}_{\rm ion}$ value that balances recombination is proportional to the clumping factor $C_{\rm HII}$, and variation in the clumping factor will also shift the required $\rho_{\rm UV}$ up or down.

4.1. *UV Luminosity Density Likelihoods*

We wish to use the evolving UV luminosity density $\rho_{\rm UV}$ to constrain the availability of ionizing photons $\dot{n}_{\rm ion}$ as given in Equation 4. Given how significantly $\rho_{\rm UV}$ increases with the limiting absolute magnitude $M_{\rm UV}$, we must evaluate the full model presented in Section 2 for chosen values of $M_{\rm UV}$. We select $M_{\rm UV} = -17$, $M_{\rm UV} = -13$, and $M_{\rm UV} = -10$ to provide a broad range of galaxy luminosities extending to extremely faint magnitudes. The observations probe to $M_{\rm UV} = -17$, and this magnitude therefore serves as a natural limit. We consider limits as faint as $M_{\rm UV} = -10$ as this magnitude may correspond to the minimum mass dark matter halo able to accrete gas from the photoheated intergalactic medium or the minimum mass dark matter halo able to retain its gas supply in the presence of supernova feedback. These scenarios have so far proven impossible to distinguish empirically (Muñoz & Loeb 2011). To make use of the constraints of the UV luminosity density on $\dot{n}_{\rm ion}$, we need to adopt a likelihood for use with

[10] When calculating whether the production rate of ionizing photons from galaxies can maintain the ionization fraction of the IGM near the end of reionization, an assumption of case A recombination is appropriate since recombinations to the hydrogen ground state largely do not help sustain the IGM ionization. For a detailed discussion, see Furlanetto & Oh (2005); Faucher-Giguère et al. (2009); Kuhlen & Faucher-Giguère (2012). We therefore adopt case A recombination in Figure 2. However, we assume case B recombination throughout the rest of the paper.

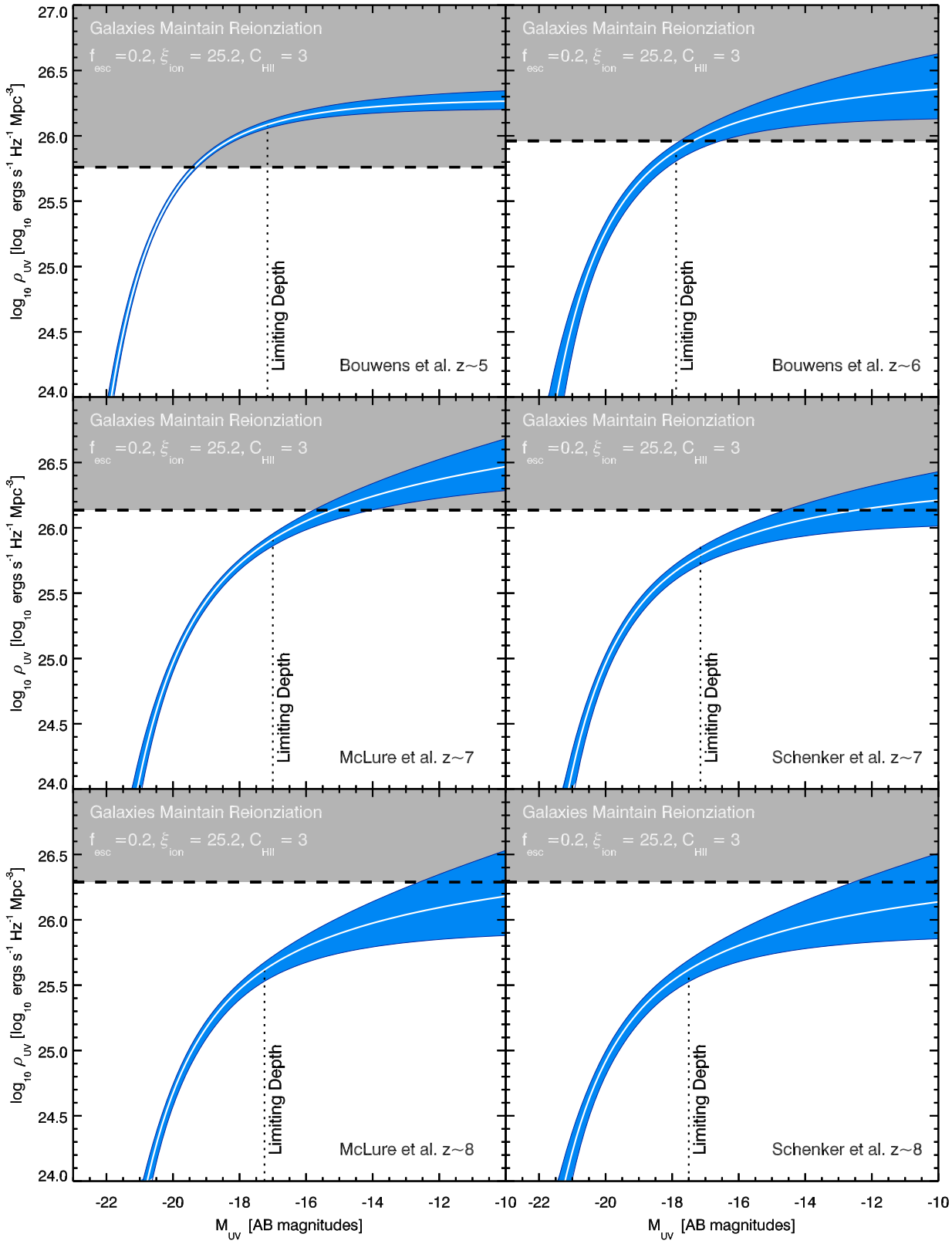

FIG. 2.— Constrained ultraviolet (UV) luminosity densities $\rho_{\rm UV}$ as a function of limiting magnitude $M_{\rm UV}$ and redshift z. Shown are the $z \sim 5-8$ maximum likelihood values of $\rho_{\rm UV}$ vs. limiting magnitude calculated using Equation 5 (white lines), and the corresponding marginalized inner 68% credibility intervals for $\rho_{\rm UV}(M_{\rm UV})$ (blue regions). In each panel, we indicate with a dotted line the limiting depth of the luminosity function determinations. Also shown is the $\rho_{\rm UV}$ required for galaxies to maintain a fully ionized universe assuming $\log \xi_{\rm ion} = 25.2$ $\log {\rm ergs}^{-1}$ Hz, $f_{\rm esc} = 0.2$, $C_{\rm HII} = 3$, and case A recombination (dashed lines and grey regions). We use Bayesian parameter estimation methods to determine the Schechter (1976) function parameter posterior distributions inferred from the stepwise maximum likelihood luminosity function (LF) data of Bouwens et al. (2007) at $z \sim 4-6$ and McLure et al. (2012) at $z \sim 7-8$. We also use the full posterior distribution sampling of the Schechter (1976) function parameters from the LF determination of Schenker et al. (2012a) to produce additional, independent constraints on $\rho_{\rm UV}$ at $z \sim 7-8$. At $z \sim 9$ where the data is limited, we simply infer the LF normalization $\phi_\star$ keeping the characteristic magnitude $M_\star$ and faint-end slope α fixed at the $z \sim 8$ values determined by McLure et al. (2012) and expect the inferred possible variation in $\rho_{\rm UV}(z \sim 9)$ to be somewhat underestimated.

Bayesian inference on parameterized forms of $\rho_{\rm UV}(z)$. Given the parameterized form of the Schechter (1976) function, we find that the marginalized posterior distributions of $\rho_{\rm UV}$ are skewed at $z \gtrsim 6$, with tails extending to larger $\log \rho_{\rm UV}$ values than a Gaussian approximation would provide. To capture this skewness, when constraining the cosmic reionization history in Section 5 below, we therefore use the full marginalized posterior distribution of $\rho_{\rm UV}$ provided by the integrated LF determinations calculated in Section 4.

Figure 3 shows the marginalized posterior distribution of the UV luminosity density $\rho_{\rm UV}$ for limiting magnitudes of $M_{\rm UV} = -17$ (red lines), $M_{\rm UV} = -13$ (orange lines), and $M_{\rm UV} = -10$ (blue lines) for our Schechter function fits to the $z \sim 5-6$ LFs of Bouwens et al. (2007), the $z \sim 7-8$ LFs of Schenker et al. (2012a), and the $z \sim 7-8$ LFs of McLure et al. (2012). Although Schenker et al. (2012a) and McLure et al. (2012) use the same data sets, their luminosity function determinations are based on different selection techniques. They therefore represent independent determinations of the high-redshift luminosity functions and are treated accordingly. We additionally use constraints from $z \sim 4$ (Bouwens et al. 2007) and $z \sim 9$ (McLure et al. 2012). The posterior distributions for $\rho_{\rm UV}(z \sim 9)$ we calculate are likely underestimated in their width owing to an assumption of fixed $M_\star$ and α values, but this assumption does not strongly influence our results. In what follows, these posterior distributions on $\rho_{\rm UV}$ are used as likelihood functions when fitting a parameterized model to the evolving UV luminosity density.

5. CONSTRAINTS ON REIONIZATION

The observational constraints on the process of cosmic reionization in the redshift range $z \gtrsim 7$ are the spectral character of high-redshift star-forming galaxies determined from the UDF12 program (Section 3 and Dunlop et al. 2012b), the evolving luminosity density constraints enabled by those same observations (Section 4, Ellis et al. 2013, Schenker et al. 2012a, and McLure et al. 2012), and the electron scattering optical depth inferred from the 9-year *WMAP* observations of the CMB (Hinshaw et al. 2012 and briefly below).

As we demonstrate, these constraints are in tension when taking the current data at face value. The Lyman continuum photon production rates per unit UV luminosity spectral density calculated using the BC03 models that are consistent with the UV spectral slopes of galaxies at $z \sim 7-9$ are $\log \xi_{\rm ion} \approx 24.8-25.3$ log ergs^{-1} Hz (Section 3), and for a reasonable escape fraction of $f_{\rm esc} \sim 0.2$ and IGM clumping factor of $C_{\rm HII}$, UV luminosity density of $\log \rho_{\rm UV} >$ 26 log ergs s^{-1} Hz^{-1} Mpc^{-3} is required to induce significant ionization at $z \geq 7$, but as we showed in Ellis et al. (2013) the observed abundance of star-forming galaxies continues a measured decline at high-redshift ($z > 8$). Further, reproducing the *WMAP* Thomson optical depth requires an extended reionization process, since instantaneous reionization ($Q_{\rm HII} = 1$) would need to occur at $z = 10.3 \pm 1.1$ to reproduce the measured $\tau = 0.084 \pm 0.013$ (Hinshaw et al. 2012) and very likely the ionization fraction $Q_{\rm HII} < 1$ at $z \gtrsim 7$. Based on the UDF12 and *WMAP* constraints, we therefore anticipate that the UV luminosity density declines to some minimum level beyond $z > 7$, and then persists with redshift to sustain a sufficient partial ionization of the IGM to satisfy the Thomson optical depth constraint. We need a methodology to quantify this process and, given its redshift dependence, to determine the required minimum luminosity of abundant star-forming galaxies to reionize the universe by $z \sim 6$.

Our chosen methodology is to use a simple parameterized model of the evolving UV luminosity density to calculate the redshift-dependent ionizing photon production rate density $\dot{n}_{\rm ion}$, constrained to reproduce the UV luminosity density values reflected by the likelihood functions shown in Figure 3. The evolving $\dot{n}_{\rm ion}$ with redshift is used to calculate the reionization history $Q_{\rm HII}(z)$ by integrating Equation 1. The corresponding Thomson optical depth is calculated using Equation 11 and then evaluated against the posterior distribution of τ provided by the public 9-year *WMAP* Monte Carlo Markov Chains. At each posterior sample evaluation, our method requires a full reconstruction of the reionization history and integration of the electron scattering optical depth and we have incorporated the reionization calculation into the *MultiNest* Bayesian inference software (Feroz & Hobson 2008; Feroz et al. 2009).

5.1. *A Parameterized Model for the Evolving UV Luminosity Density*

To infer constraints on the reionization process, we must adopt a flexible parameterized model for the evolving UV luminosity density. The model must account for the decline of $\rho_{\rm UV}$ apparent in Figures 2 and 3, without artificially extending the trend in $\rho_{\rm UV}$ at $z \lesssim 6$ to redshifts $z \gtrsim 8$. The rapid decline in $\rho_{\rm UV}$ between $z \sim 4$ and $z \sim 5$ suggests a trend of $d\log\rho_{\rm UV}/d\log z \sim -3$, but the higher redshift values of $\rho_{\rm UV}$ flatten away from this trend, especially for faint limiting magnitudes. Beyond $z \sim 10$, we expect that some low-level UV luminosity density will be required to reproduce the Thomson optical depth, to varying degrees depending on the chosen limiting magnitude.

With these features in mind, we have tried a variety of parameterized models for $\rho_{\rm UV}$. We will present constraints using a three-parameter model given by

$$\rho_{\rm UV}(z) = \rho_{\rm UV,z=4}\left(\frac{z}{4}\right)^{-3} + \rho_{\rm UV,z=7}\left(\frac{z}{7}\right)^{\gamma}. \qquad (14)$$

The low-redshift amplitude of this model is anchored by the UV luminosity density at $z \sim 4$, $\rho_{\rm UV,z=4}$ with units of ergs s^{-1} Hz^{-1} Mpc^{-3}. The high-redshift evolution is determined by the normalization $\rho_{\rm UV,z=7}$ at $z \sim 7$, provided in units of ergs s^{-1} Hz^{-1} Mpc^{-3}, and the power-law slope γ. Using this model, we compute the evolving $\rho_{\rm UV}(z)$ and evaluate the parameter likelihoods as described immediately above.

We have examined other models, including general broken (double) power-laws and low-redshift power-laws with high-redshift constants or fixed slope power-laws. Single power-law models tend to be dominated by the low-redshift decline in the $\rho_{\rm UV}$ and have difficulty reproducing the Thomson optical depth. Generic broken power-law models have a degeneracy between the low- and high-redshift evolution, even for fixed redshifts about which the power laws are defined, and are disfavored based on their Bayesian information relative to less complicated models that can also reproduce the $\rho_{\rm UV}$ constraints. The model in Equation 14 is therefore a good compromise between sufficient generality and resulting parameter degeneracies.

However, when using this model, we use a prior to limit $\gamma < 0$ to prevent *increasing* $\rho_{\rm UV}$ beyond $z \sim 9$. The best current constraints on the abundance of $z > 8.5$ galaxies is from Ellis et al. (2013), where we demonstrated that the highest-redshift galaxies (with $M_{\rm UV} \lesssim -19$) continue the smooth decline in abundance found at slightly later times. Correspond-

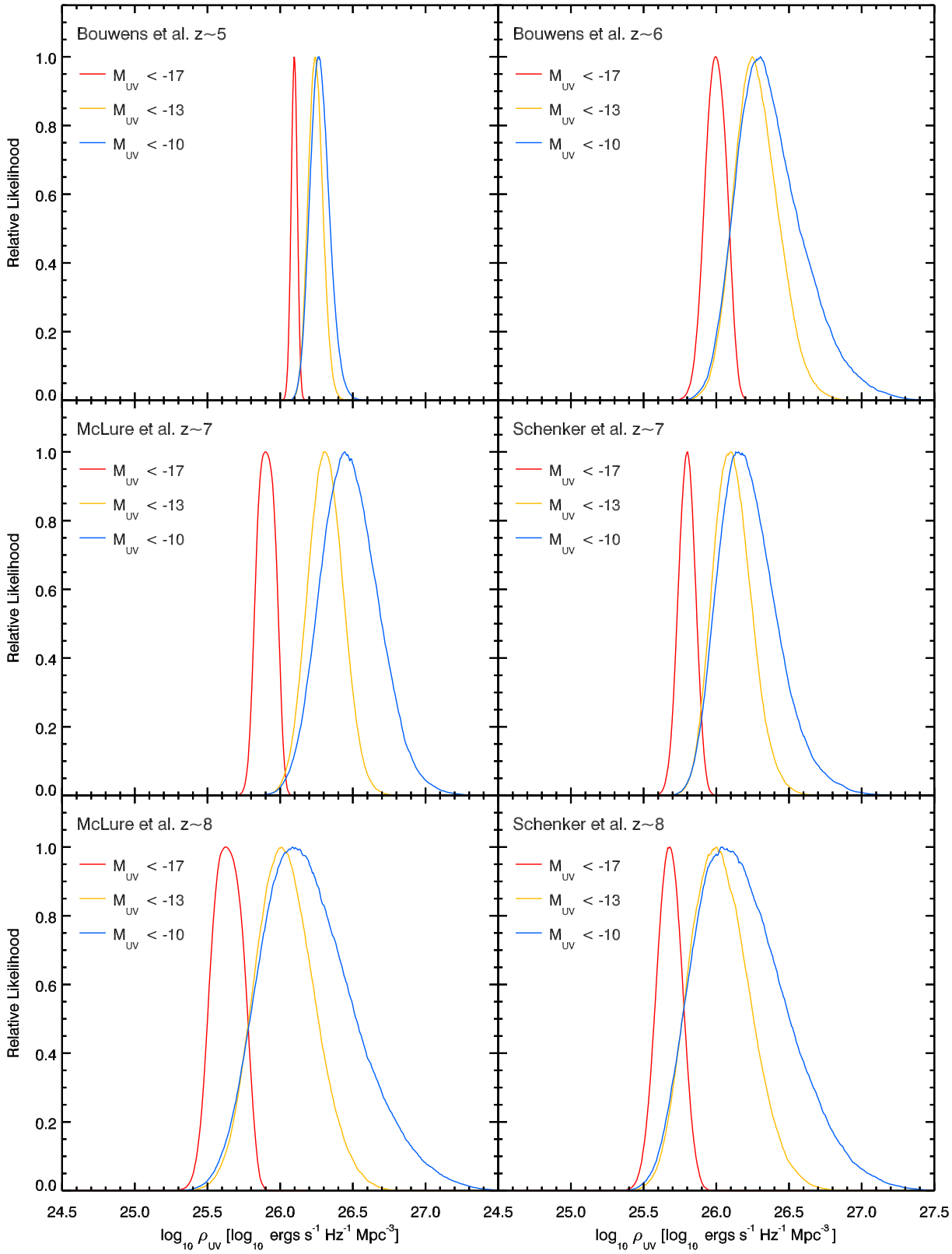

FIG. 3.— Likelihood functions of the UV luminosity density $\rho_{\rm UV}$ for different limiting magnitudes and redshifts used to constrain the reionization history. Shown are the $z \sim 5-8$ marginalized posterior distributions for $\rho_{\rm UV}$ determined from Schechter (1976) function fits to luminosity function (LF) data, as reported in Figure 2, for limiting magnitudes of $M_{\rm UV} < -17$ (red lines), $M_{\rm UV} < -13$ (orange lines), and $M_{\rm UV} < -10$ (blue lines). To infer the distributions at $z \sim 4-9$, we use the LF data of Bouwens et al. (2007) at $z \sim 4-6$, McLure et al. (2012) at $z \sim 7-9$, and Schenker et al. (2012a) at $z \sim 7-8$. In our posterior distributions for $\rho_{\rm UV}(z \sim 9)$, we keep the characteristic magnitude $M_\star$ and faint-end-slope α values fixed at the $z \sim 8$ best fit values reported by McLure et al. (2012) but expect the width of distribution to be somewhat overly narrow. These posterior distributions on $\rho_{\rm UV}$ are used as likelihood functions when fitting a parameterized model to the evolving UV luminosity density.

ingly, the constraint on γ amounts to a limit on introducing a new population of galaxies arising at $z \gtrsim 9$. The usefulness of this potentiality for the reionization of the universe has been noted elsewhere (e.g., Cen 2003; Alvarez et al. 2012). While imposing no constraint besides $\gamma < 0$, we typically find that nearly constant, low-level luminosity densities at high-redshift are nonetheless favored (see below). Results for models that feature low-redshift power-law declines followed by low-level constant $\rho_{\rm UV}$ at high-redshift will produce similar quantitative results. All parameterized models we have examined that feature a declining or constant $\rho_{\rm UV}$ and can reproduce the Thomson optical depth constraint produce similar results, and we conclude that our choice of the exact form of Equation 14 is not critical.

5.2. *Reionization Constraints from Galaxies*

Figure 4 shows constraints on the reionization process calculated using the model described in Section 2. We perform our Bayesian inference modeling assuming $M_{\rm UV} < -17$ (close to the UDF12 limit at $z \sim 8$, maximum likelihood model is shown as a dashed line in all panels), $M_{\rm UV} < -10$ (an extremely faint limit, with the maximum likelihood model shown as a dotted line in all panels), and an intermediate limit $M_{\rm UV} < -13$ (colored regions show 68% credibility regions, while white lines indicate the maximum likelihood model). We now will discuss the UV luminosity density, stellar mass density, ionized filling fraction, and electron scattering optical depth results in turn.

The upper left hand panel shows parameterized models of the UV luminosity density (as given in Equation 14), constrained by observations of the UV luminosity density (inferred from the measured luminosity functions, see Figures 2 and 3) integrated down to each limiting magnitude. The figure shows error bars to indicate the 68% credibility width of the posterior distributions of $\rho_{\rm UV}$ at redshifts $z \sim 4-9$ integrated to $M_{\rm UV} < -13$, but the likelihood of each model is calculated using the full marginalized $\rho_{\rm UV}$ posterior distributions appropriate for its limiting magnitude. In each case the $\rho_{\rm UV}(z)$ evolution matches well the constraints provided by the luminosity function extrapolations, which owes to the well-defined progression of declining $\rho_{\rm UV}$ with redshift inferred from the UDF12 and earlier datasets. For reference, the maximum likelihood values for the parameters of Equation 14 for $M_{\rm UV} < -13$ are log $\rho_{{\rm UV},z=4} = 26.50$ log ergs s^{-1} Hz^{-1} Mpc^{-3}, log $\rho_{{\rm UV},z=7} = 25.82$ log ergs s^{-1} Hz^{-1} Mpc^{-3}, and $\gamma = -0.003$.

What drives the constraints on $\rho_{\rm UV}$ for these limiting magnitudes? Some tension exists at high-redshift, as the models prefer a relatively flat $\rho_{\rm UV}(z)$ beyond the current reach of the data. In each case, the maximum likelihood models become flat at high-redshift and reflect the need for continued star formation at high-redshift to sustain a low-level of partial IGM ionization. To better answer this question, we have to calculate the full stellar mass density evolutions, reionization histories, and Thomson optical depths of each model.

The lower left hand panel shows how the models compare to the stellar mass densities extrapolated from the results by Stark et al. (2012), using the method described in Section 2. The error bars in the figure reflect the stellar mass densities extrapolated for contributions from galaxies with $M_{\rm UV} < -13$, but the appropriately extrapolated mass densities are used for each model. The error bars reflect bootstrap-calculated uncertainties that account for statistically possible variations in the best fit stellar mass - UV luminosity relation given by Equation 8, and are $\sigma \approx 0.3$ dex at $z \sim 7$. To balance the relative constraint from the stellar mass density evolution with the single optical depth constraint (below), we assign the likelihood contributions of the stellar mass density and Thomson optical depth equal weight. The stellar mass densities calculated from the models evolve near the $1-\sigma$ upper limits of the extrapolated constraints, again reflecting the need for continued star formation to sustain a low-level of IGM ionization.[11]

Assuming a ratio of Lyman continuum photon production rate to UV luminosity $\log \xi_{\rm ion} = 25.2$ log ergs^{-1} Hz for individual sources consistent with UV slopes measured from the UDF12 data (Dunlop et al. 2012b), an ionizing photon escape fraction $f_{\rm esc} = 0.2$, and an intergalactic medium clumping factor of $C_{\rm HII} = 3$, the reionization history $Q_{\rm HII}(z)$ produced by the evolving $\rho_{\rm UV}$ can be calculated by integrating Equation 1 and is shown in the upper right panel of Figure 4. We find that the currently observed galaxy population at magnitudes brighter than $M_{\rm UV} < -17$ (dashed line) can only manage to reionize fully the universe at late times $z \sim 5$, with the IGM 50% ionized by $z \sim 6$ and < 5% ionized at $z \sim 12$. Contributions from galaxies with $M_{\rm UV} < -13$ reionize the universe just after $z \sim 6$, in agreement with a host of additional constraints on the evolving ionized fraction (see Section 6 below) and as suggested by some previous analyses (e.g., Salvaterra et al. 2011). These galaxies can sustain a ~ 50% ionized fraction at $z \sim 7.5$, continuing to $\sim 12-15$% at redshift $z \sim 12$. Integrating further down to $M_{\rm UV} < -10$ produces maximum likelihood models that reionize the universe slightly earlier.

The Thomson optical depths resulting from the reionization histories can be determined by evaluating Equation 11. To reproduce the 9-Year *WMAP* τ values, most models display low levels of UV luminosity density that persist to high redshift. Even maintaining a flat $\rho_{\rm UV}$ at the maximum level allowed by the luminosity density constraints at redshifts $z \lesssim 9$, as the maximum likelihood models do, the optical depth just can be reproduced. When considering only the currently observed population $M_{\rm UV} < -17$, the UV luminosity density would need to increase toward higher $z > 10$ redshifts for the universe to be fully reionized by redshift $z \sim 6$ and the Thomson optical depth to be reproduced.

We remind the reader that while the exact results for, e.g., the $Q_{\rm HII}$ evolution of course depends on the choices for the escape fraction $f_{\rm esc}$ or the ionizing photon production rate $\xi_{\rm ion}$. If $f_{\rm esc}$ or $\xi_{\rm ion}$ are lowered, the evolution of $Q_{\rm HII}$ is shifted toward lower redshift. For instance, with all other assumptions fixed, we find that complete reionization is shifted to $z \sim 5$ for $f_{\rm esc} = 0.1$ and $z \sim 4.75$ for log $\xi_{\rm ion} = 25.0$ log ergs^{-1} Hz. Complete reionization can also be made earlier by choosing a smaller $C_{\rm HII}$ or delayed by choosing a larger $C_{\rm HII}$.

Given the above results, we conclude that under our assumptions (e.g., $f_{\rm esc} = 0.2$ and $C_{\rm HII} \approx 3$) galaxies currently observed down to the limiting magnitudes of deep high-redshift surveys (e.g., UDF12) do not reionize the universe alone, and to simultaneously reproduce the $\rho_{\rm UV}$ constraints, the τ constraint, and to reionize the universe by $z \sim 6$ requires yet fainter populations. This conclusion is a ramification of the UDF12 UV spectral slope constraints by Dunlop et al.

[11] We note that if we ignore the electron scattering optical depth constraint, the other datasets favor a UV luminosity density that declines more rapidly at high redshift than does our maximum likelihood model calculated including all the constraints. However, the UV luminosity density parameters in Equation 14 remain similar. Excluding the stellar mass density constraint has almost no effect on the maximum likelihood parameters inferred for the model.

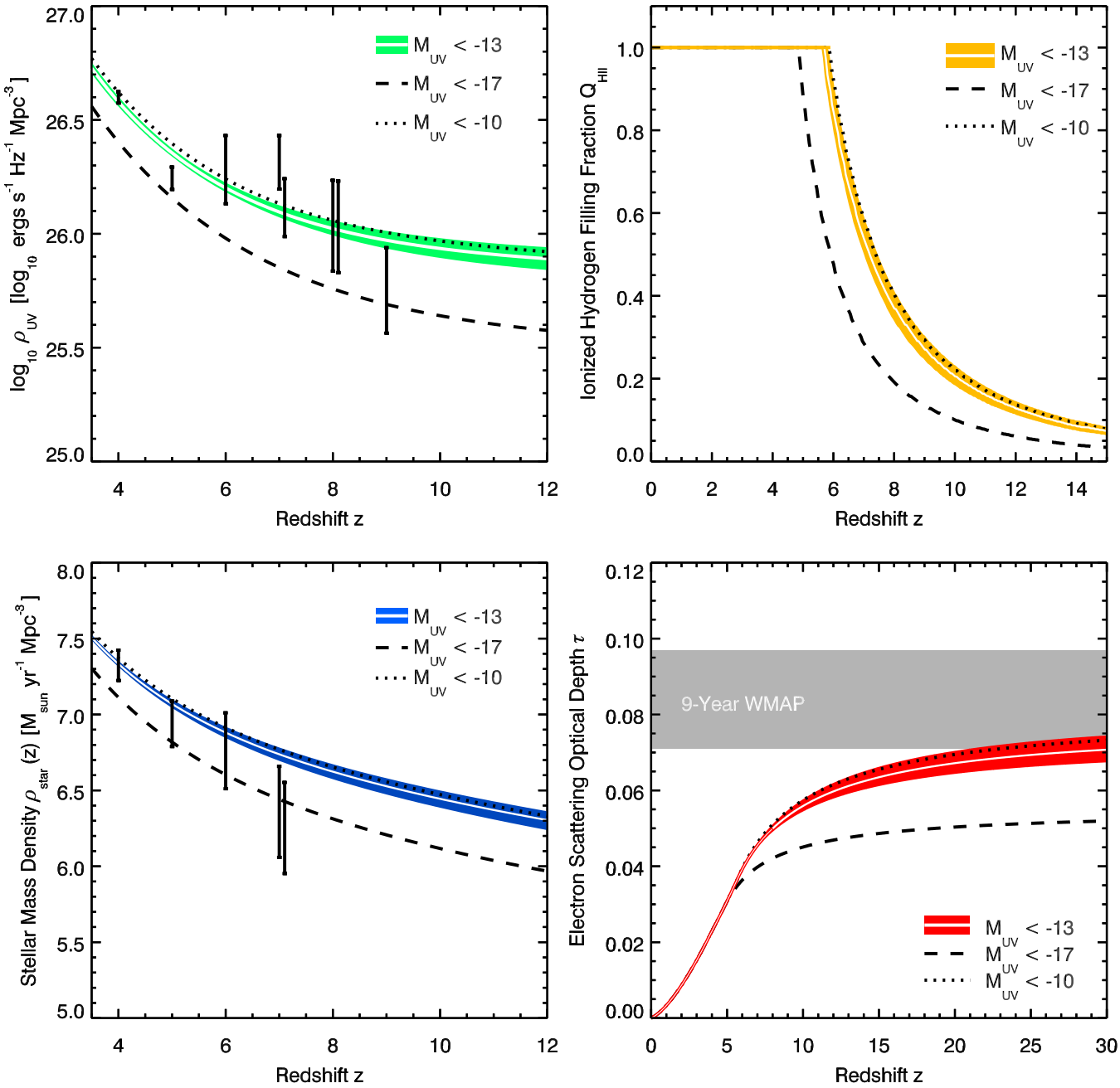

FIG. 4.— Joint constraints on the reionization history, assuming ionizing photon contributions from galaxies with $M_{\rm UV} < -17$ (maximum likelihood model shown as dashed line in all panels), $M_{\rm UV} < -10$ (maximum likelihood model shown as dotted line in all panels), and $M_{\rm UV} < -13$ (maximum likelihood model shown as white line in all panels; 68% credibility regions shown as colored areas). We use the posterior distributions for $\rho_{\rm UV}$ with redshift shown in Figure 3, extrapolated stellar mass density constraints, and the posterior distribution on the electron scattering optical depth (Hinshaw et al. 2012) as likelihood functions to constrain the simple parameterized model for the evolving UV luminosity density given by Equation 14 at redshifts $z \gtrsim 4$. The constrained evolution of $\rho_{\rm UV}$ is shown in the upper left panel (error bars indicate the $\rho_{\rm UV}$ constraints for $M_{\rm UV} < -13$, but each model uses the appropriate constraints). From $\rho_{\rm UV}(z)$, we can simply integrate with redshift to determine the stellar mass densities (bottom left panel; data points with error bars indicate extrapolations of the Stark et al. (2012) stellar mass densities to $M_{\rm UV} < -13$, but all models use the appropriate constraints). The models tend to exceed slightly the stellar mass densities at the highest-redshifts ($z \sim 7$), a result driven by the constraint on the election scattering optical depth. By assuming the well-motivated values of the ratio of Lyman continuum photon production rate to UV luminosity $\log \xi_{\rm ion} = 25.2$ $\log$ ergs^{-1} Hz for individual sources, an ionizing photon escape fraction $f_{\rm esc} = 0.2$, and an intergalactic medium clumping factor of $C_{\rm HII} = 3$, the reionization history $Q_{\rm HII}$ calculated by integrating Equation 1 is shown in the upper right panel. Integrating the reionization history provides the electron scattering optical depth (lower right panel, 9-year *WMAP* constraint indicated as the grey region).

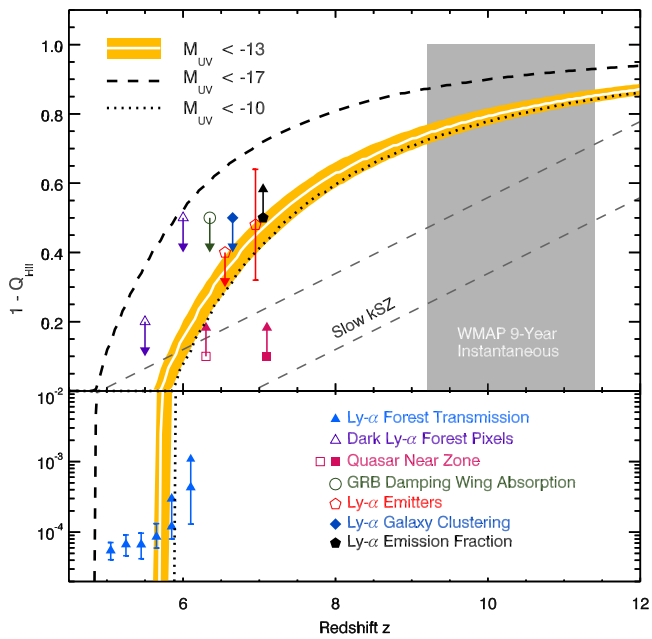

FIG. 5.— Reionization histories for models that include galaxies with $M_{\rm UV} < -13$ (maximum likelihood model: white line; 68% credibility region: orange area), $M_{\rm UV} < -17$ (maximum likelihood model only, dashed line), and $M_{\rm UV} < -10$ (maximum likelihood model only, dotted line). We also show a collection of other claimed constraints on the neutral fraction $1-Q_{\rm HII}$; note how the ordinate switches from log to linear to more clearly illustrate the full range of measurements. These include (see text for details and references): measurements of the Lyman-α forest transmission (blue solid triangles), conservative upper limits on the neutral fraction from the fraction of dark pixels in the Lyman-α forest (purple open triangles), quasar near-zone measurements (open and solid magenta squares), damping wing absorption in a GRB (open green circle), the evolving abundance of Lyman-α emitter galaxies (open red pentagons), the clustering of those galaxies (filled dark blue diamond), and the evolving fraction of Lyman-break galaxies with strong Lyman-α emission lines (filled black pentagon). The grey dashed lines labeled "Slow kSZ" are purely illustrative, showing the slowest evolution currently allowed by the small-scale CMB temperature data; the endpoint of reionization is arbitrary in these cases. Finally, the shaded gray region shows the redshift during which instantaneous reionization would occur according to the WMAP 9-year data.

(2012b), which eliminate the possibility that increased Lyman continuum emission by metal-poor populations could have produced reionization at $z > 6$ (e.g., Robertson et al. 2010). However, too much additional star formation beyond the $M_{\rm UV} < -13$ models shown in Figure 4 will begin to exceed the stellar mass density constraints, depending on $f_{\rm esc}$. It is therefore interesting to know whether the $M_{\rm UV} < -13$ models that satisfy the $\rho_{\rm UV}$, $\rho_\star$, and τ constraints also satisfy other external constraints on the reionization process, and we now turn to such an analysis.

6. COMPARISON TO OTHER PROBES OF THE IONIZED FRACTION

In this section we will collect constraints on the IGM neutral fraction from the literature and compare them to the evolution of this quantity in our models based on the UDF12 data. These constraints come from a wide variety of astrophysical measurements, but all are subject to substantial systematic or modeling uncertainties, about which we will comment below. We show the full set in Figure 5, along with a comparison to our model histories. We will first briefly discuss these constraints and then how our model histories fare in comparison to them.

6.1. *The Lyman-α Forest*

The best known Lyman-α forest constraints come from Fan et al. (2006b), who measured the effective optical depth evolution along lines of sight taken from SDSS (including both Lyman-α and higher-order transitions, where available). Those authors then made assumptions about the IGM temperature and the distribution of density inhomogeneities throughout the universe to infer the evolution of the neutral fraction (these assumptions are necessary for comparing the higher-order transitions to Lyman-α as well, because those transitions sample different parts of the IGM). The corresponding limits on the neutral fraction according to their model are shown by the filled triangles in Figure 5.

The original data here are the transmission measurements in the different transitions. Transforming those into constraints on the ionized fraction requires a model that: (1) predicts the temperature evolution of the IGM (Hui & Haiman 2003; Trac et al. 2008; Furlanetto & Oh 2009); (2) describes the distribution of gas densities in the IGM (Miralda-Escudé et al. 2000; Bolton & Becker 2009); (3) accounts for spatial structure in the averaged transmission measurements (Lidz et al. 2006); and (4) predicts the topology of ionized and neutral regions at the tail end of reionization (Furlanetto et al. 2004b; Choudhury et al. 2009). These are all difficult, and the Fan et al. (2006b) constraints – based upon a simple semi-analytic model for the IGM structure – can be evaded in a number of ways. In particular, their model explicitly ignores the possibility that $Q_{\rm HII} < 1$, working only with the residual neutral gas inside a mostly ionized medium.

Unsurprisingly, our models do not match these Lyman-α forest measurements very well. The crude approach of Equation 1 fails to address effects from the detailed density structure of the IGM on the evolution of the mean ionization fraction near the end of the reionization process. Our model is therefore not sufficient to model adequately the tail end of reionization, and only more comprehensive models that account for both radiative transfer effects and the details of IGM structure will realistically model these data at $z < 6$.

More useful to us is a (nearly) model-independent *upper* limit on the neutral fraction provided by simply counting the dark pixels in the spectra (Mesinger 2010). McGreer et al. (2011) present several different sets of constraints, depending on how one defines "dark" and whether one uses a small number of very deep spectra (with a clearer meaning to the dark pixels but more cosmic variance) versus a larger set of shallower spectra. Their strongest constraints are roughly $1-Q_{\rm HII} < 0.2$ at $z = 5.5$ and $1-Q_{\rm HII} < 0.5$ at $z = 6$, shown by the open triangles in Figure 5. Interestingly, this model-independent approach permits rather late reionization.

6.2. *Ionizing Background*

Another use of the Lyman-α forest is to measure the ionizing background and thereby constrain the emissivity ϵ of galaxies: the ionization rate $\Gamma \propto \epsilon\lambda$, where λ is the Lyman continuum mean free path. Bolton & Haehnelt (2007b) attempted such a measurement at $z > 5$. The method is difficult as it involves interpretation of spectra near the saturation limit of the forest. Nonetheless, the Bolton & Haehnelt (2007b) analysis shows that the ionizing background falls by about a factor of ten from $z \sim 3$ to to $z \sim 6$ (though see McQuinn et al. 2011). The resulting comoving emissivity is roughly the same as at $z \sim 2$, corresponding to 1.5–3 photons per hydrogen atom over the age of the Universe (see also Haardt & Madau 2012).

Additional detailed constraints were derived by Faucher-Giguère et al. (2008), who used quasar spectra at $2 \lesssim z \lesssim 4$ to infer a photoionization rate for intergalactic hydrogen. Combining these measurements with the previous work by Bolton & Haehnelt (2007b) and estimates of the intergalactic mean free path of Lyman continuum photons (Prochaska et al. 2009; Songaila & Cowie 2010), Kuhlen & Faucher-Giguère (2012) calculated constraints on the comoving ionizing photon production rate. These inferred values of $\log \dot{n}_{\rm ion} < 51$ $\log$ s^{-1} Mpc^{-3} at $z \sim 2-6$ are lower than those produced by naively extrapolating typical models of the evolving high-redshift UV luminosity density that satisfy reionization constraints. To satisfy both the low-redshift IGM emissivity constraints and the reionization era constraints then available, Kuhlen & Faucher-Giguère (2012) posited an evolving escape fraction

$$f_{\rm esc}(z) = f_0 \times [(1+z)/5]^{\kappa}. \quad (15)$$

If the power-law slope κ is large enough, the IGM emissivity constraints at $z < 6$ can be satisfied with a low f_0 while still reionizing the universe by $z \sim 6$ and matching previous *WMAP* constraints on the electron scattering optical depth. Other previous analyses have emphasized similar needs for an evolving escape fraction (e.g., Ferrara & Loeb 2012; Mitra et al. 2013).

To study the effects of including the IGM emissivity constraints by permitting an evolving $f_{\rm esc}$, we repeat our calculations in Section 5 additionally allowing an escape fraction given by Equation 15 with varying f_0 and κ (and maximum escape fraction $f_{\rm max} = 1$). With a limiting magnitude $M_{\rm UV} < -13$, and utilizing the updated constraints from UDF12 and *WMAP*, we find maximum likelihood values $f_0 = 0.054$ and $\kappa = 2.4$ entirely consistent with the results of Kuhlen & Faucher-Giguère (2012, see their Figure 7). When allowing for this evolving $f_{\rm esc}$ (with $f_{\rm max} = 1$), we sensibly find that the need for low-level star formation to satisfy reionization constraints is reduced (the maximum likelihood model has a high-redshift luminosity density evolution of $\rho_{\rm UV} \propto z^{-1.2}$) and the agreement with the stellar mass density constraints is improved.

However, the impact of the evolving $f_{\rm esc}(z)$ depends on the maximum allowed $f_{\rm esc}$. We allow only $f_{\rm esc}$ to vary (not the product $f_{\rm esc}\xi_{\rm ion}$) owing to our UV spectral slope constraints, and the maximum $f_{\rm esc} = 1$ (and, correspondingly, the maximum ionizing photon production rate per galaxy) is reached by $z \sim 15$. In this model with maximum $f_{\rm max} = 1$, the escape fraction at $z \sim 7-8$ (where the ionized volume filling factor $Q_{\rm HII}$ is changing rapidly) is $f_{\rm esc} \sim 0.17-0.22$, very similar to our fiducial constant $f_{\rm esc} = 0.2$ adopted in Section 5. The rate of escaping ionizing photons per galaxy in this evolving $f_{\rm esc}$ model with maximum $f_{\rm max} = 1$ trades off against the high-redshift UV luminosity density evolution. The need for a low-level of star formation out to high redshift is somewhat reduced as the increasing escape fraction with redshift compensates to maintain a partial IGM ionization fraction and recover the observed *WMAP* τ. Without placing additional constraints on the end of reionization, this evolving $f_{\rm esc}$ model with $f_{\rm max} = 1$ produces a broader redshift range of $z \sim 4.5-6.5$ for the completion of the reionization process than the constant $f_{\rm esc}$ model described in Section 5.

If we instead adopt an evolving $f_{\rm esc}$ model with $f_{\rm max} = 0.2$ we recover $\rho_{\rm UV}$, $\rho_\star$, and Thomson optical depth evolutions that are similar to the constant $f_{\rm esc}$ model from Section 5, but can also satisfy the additional low-redshift IGM emissivity constraints. Compared with the comoving ionizing photon production rates $\dot{n} = [3.2, 3.5, 4.3] \times 10^{50}$ s^{-1} Mpc^{-3} at redshifts $z = [4.0, 4.2, 5.0]$ inferred by Kuhlen & Faucher-Giguère (2012) from measurements by Faucher-Giguère et al. (2008), Prochaska et al. (2009), and Songaila & Cowie (2010), this maximum likelihood model with evolving $f_{\rm esc}$ recovers similar values ($\dot{n} = [3.3, 3.5, 4.7] \times 10^{50}$ s^{-1} Mpc^{-3} at $z = [4, 4.2, 5]$). In contrast, the constant $f_{\rm esc}$ model in Section 5 calculated without consideration of these IGM emissivity constraints would produce $\dot{n} \sim 8-13 \times 10^{50}$ s^{-1} Mpc^{-3} at $z \sim 4-5$. The reduction of the escape fraction at $z \sim 4-6$ compared with the baseline model with constant $f_{\rm esc}$ allows full ionization of the IGM to occur slightly later in the evolving $f_{\rm esc}$ model (at redshifts as low as $z \approx 5.3$, although in the maximum likelihood model reionization completes within $\Delta z \approx 0.1$ of the redshift suggested by the maximum likelihood constant $f_{\rm esc}$ model of Section 5).

With a similar range of assumptions to Kuhlen & Faucher-Giguère (2012) for a time-dependence in the escape fraction, the model presented in Section 5 can therefore also satisfy the low-redshift IGM emissivity constraints without assuming an escape fraction of $f_{\rm esc} \sim 1$ at high redshifts. While the evolving covering fraction in galaxy spectra (Jones et al. 2012) provides additional observational support for a possible evolution in the escape fraction at $z \lesssim 5$, such empirical support for evolving $f_{\rm esc}$ does not yet exist at $z \gtrsim 5$.

6.3. *The Lyman-α Damping Wing*

Another use of the Lyman-α line is to measure precisely the shape of the red damping wing of the line: the IGM absorption is so optically thick that the shape of this red absorption wing depends upon the mean neutral fraction in the IGM (Miralda-Escudé 1998), though the interpretation depends upon the morphology of the reionization process, leading to large intrinsic scatter and biases (McQuinn et al. 2008; Mesinger & Furlanetto 2008a). Such an experiment requires a deep spectrum of a bright source in order to identify the damping wing.

One possibility is a gamma-ray burst, which has an intrinsic power-law spectrum, making it relatively easy to map the shape of a damping wing. The disadvantage of these sources is that (at lower redshifts) they almost always have damped Lyman-α (DLA) absorption from the host galaxy, which must be disentangled from any IGM signal (Chen et al. 2007).

To date, the best example of such a source is GRB050904 at $z = 6.3$, which received rapid followup and produced a high signal-to-noise spectrum (Totani et al. 2006). McQuinn et al. (2008) studied this spectrum in light of patchy reionization models. Because it has intrinsic DLA absorption, the constraints are relatively weak: they disfavor a fully neutral IGM but allow $Q_{\rm HII} \sim 0.5$. We show this measurement with the open circle in Figure 5.

Quasars provide a second possible set of sources. These are much easier to find but suffer from complicated intrinsic spectra near the Lyman-α line. Schroeder et al. (2012) have modeled the spectra of three SDSS quasars in the range $z = 6.24$–6.42 and found that all three are best fit if a damping wing is present (see also Mesinger & Haiman 2004). Although the spectra themselves cannot distinguish an IGM damping wing from a DLA, they argue that the latter should be sufficiently rare that the IGM must have $Q_{\rm HII} \lesssim 0.1$ at 95% confidence.

We show this point as the open square in Figure 5. This conclusion is predicated on accurate modeling of the morphology of reionization around quasars and the distribution of strong IGM absorbers at the end of reionization.

6.4. *The Near Zones of Bright Quasars*

Any ionizing source that turns on inside a mostly neutral medium will carve out an H II region whose extent depends upon the total fluence of ionizing photons from the source. If one can measure (or guess) this fluence, the extent of the ionized bubble then offers a constraint on the original neutral fraction of the medium. This is, of course, a difficult proposition, as the extremely large Lyman-α IGM optical depth implies that the spectrum may go dark even if the region is still highly-ionized: in this case, you find only a lower limit to the size of the near zone (Bolton & Haehnelt 2007a).

Carilli et al. (2010) examined the trends of near-zone sizes in SDSS quasars from z = 5.8–6.4. The sample shows a clear trend of decreasing size with increasing redshift (after compensation for varying luminosities) by about a factor of two over that redshift range. Under the assumption that near zones correspond to ionized bubbles in a (partially) neutral medium, the volume $V \propto (1-Q_{\rm HII})^{-1}$, or, in terms of the radius, $R_{\rm NZ}^{-3} \propto (1-Q_{\rm HII})$. In that case, a two-fold decrease in size corresponds to an order of magnitude increase in the neutral fraction. However, if the Fan et al. (2006b) Lyman-α forest measurements are correct, the neutral fraction at $z \sim 5.8$ is so small that the zones are very unlikely to be in this regime. In that case, the trend in sizes cannot be directly transformed into a constraint on the filling factor of ionized gas. We therefore do not show this constraint on Figure 5, as its interpretation is unclear.

The recently discovered z = 7.1 quasar has a very small near-zone (Mortlock et al. 2011). Bolton et al. (2011) used a numerical simulation to analyze it in detail. They concluded the spectrum was consistent both with a small ionized bubble inside a region with $Q_{\rm HII} \lesssim 0.1$ and with a highly-ionized medium $(1-Q_{\rm HII}) \sim 10^{-4}$–$10^{-3}$ if a DLA is relatively close to the quasar. They argue that the latter is relatively unlikely (occurring $\sim$ 5% of the time in their simulations). Further support to the IGM hypothesis is lent by recent observations showing no apparent metals in the absorber, which would be unprecedented for a DLA (Simcoe et al. 2012). A final possibility is that the quasar is simply very young ($\lesssim 10^6$ yr) and has not had time to carve out a large ionized region. We show this constraint, assuming that the absorption comes from the IGM, with the filled square in Figure 5.

6.5. *The Kinetic Sunyaev-Zel'dovich Effect*

Recent small-scale temperature measurements have begun to constrain the contribution of patchy reionization to the kinetic Sunyaev-Zel'dovich (kSZ) effect, which is generated by CMB photons scattering off coherent large-scale velocities in the IGM. These scatterings typically cancel (because any redshift gained from scattering off of gas falling into a potential well is canceled by scattering off gas on the other side), but during reionization modulation by the ionization field can prevent such cancellation (Gruzinov & Hu 1998; Knox et al. 1998). There is also a contribution from nonlinear evolution, see Ostriker & Vishniac (1986). Both the Atacama Cosmology Telescope and the South Pole Telescope have placed upper limits on this signal (Dunkley et al. 2011; Reichardt et al. 2012).

Because the patchiness and inhomogeneity of the process induce this signal, the kSZ signal grows so long as this patchy contribution persists. As a result, it essentially constrains the duration of reionization. Using SPT data, Zahn et al. (2012) claim a limit of $\Delta z < 7.2$ (where Δz is the redshift difference between $Q_{\rm HII}$ = 0.2 and $Q_{\rm HII}$ = 0.99) at 95% confidence. The primary limiting factor here is a potential correlation between the thermal Sunyaev-Zel'dovich effect and the cosmic infrared background, which pollutes the kSZ signal. If that possibility is ignored, the limit on the duration falls to $\Delta z < 4.4$. Mesinger et al. (2012) found similar limits from ACT data. They showed that the limit without a correlation is difficult to reconcile with the usual models of reionization. Intensive efforts are now underway to measure the correlation.

We show two examples of the *slowest* possible evolution allowed by these constraints (allowing for a correlation) with the straight dashed lines in Figure 5. Note that the timing of these curves is entirely arbitrary (as is the shape: there is absolutely no reason to expect a linear correlation between redshift and neutral fraction). They simply offer a rough guide to the maximum duration over which substantial patchiness can persist.

6.6. *Lyman-α Lines in Galaxies*

The final class of probes to be considered here relies on Lyman-α emission lines from galaxies (including some of those cataloged in the HUDF09 and UDF12 campaigns). As these line photons propagate from their source galaxy to the observer, they pass through the IGM and can suffer absorption if the medium has a substantial neutral fraction. This absorption is generally due to the red damping wing, as the sources most likely lie inside of ionized bubbles, so the line photons have typically redshifted out of resonance by the time they reach neutral gas.

One set of constraints come from direct (narrowband) surveys for Lyman-α emitting galaxies. As the IGM becomes more neutral, these emission lines should suffer more and more extinction, and so we should see a drop in the number density of objects selected in this manner (Santos 2004; Furlanetto et al. 2004a, 2006; McQuinn et al. 2007; Mesinger & Furlanetto 2008b). Such surveys have a long history (e.g., Hu et al. 2002; Malhotra & Rhoads 2004; Santos et al. 2004; Kashikawa et al. 2006). To date, the most comprehensive surveys have come from the Subaru telescope. Ouchi et al. (2010) examined z = 6.6 Lyman-α emitters and found evidence for only a slight decline in the Lyman-α transmission. They estimate that $Q_{\rm HII} \gtrsim 0.6$ at that time. Ota et al. (2008) examined the z = 7 window. Very few sources were detected, which may indicate a rapid decline in the population. They estimate that $Q_{\rm HII} \approx 0.32$–0.64. We show these two constraints with the open pentagons in Figure 5.

The primary difficulty with measurements of the evolution of the Lyman-α emitter number density is that the overall galaxy population is also evolving, and it can be difficult to determine if evolution in the emitter number counts is due to changes in the IGM properties or in the galaxy population. An alternate approach is therefore to select a galaxy sample independently of the Lyman-α line (or at least as independently as possible) and determine how the fraction of these galaxies with strong Lyman-α lines evolves (Stark et al. 2010). Such a sample is available through broadband Lyman break searches with HST and Subaru. Several groups have performed these searches to $z \sim 8$ (Fontana et al. 2010; Pentericci et al. 2011; Schenker et al. 2012b; Ono et al.

2012b) and found that, although the fraction of Lyman-α emitters increases slightly for samples of similar UV luminosity from $z \sim 3$–6, there is a marked decline beyond $z \sim 6.5$ (see also Treu et al. 2012). This decline could still be due to evolutionary processes within the population (e.g., dust content, see Dayal & Ferrara 2012), but both the rapidity of the possible evolution and its reversal from trends now well-established at lower redshift make this unlikely. Assuming that this decline can be attributed to the increasing neutrality of the IGM, it requires $Q_{\rm HII} \lesssim 0.5$ (McQuinn et al. 2007; Mesinger & Furlanetto 2008b; Dijkstra et al. 2011). We show this constraint with the filled pentagon in Figure 5.

There is one more signature of reionization in the Lyman-α lines of galaxies. A partially neutral IGM does not extinguish these lines uniformly: galaxies inside of very large ionized bubbles suffer little absorption, while isolated galaxies disappear even when $Q_{\rm HII}$ is large. This manifests as a change in the apparent clustering of the galaxies, which is attractive because such a strong change is difficult to mimic with baryonic processes within and around galaxies (Furlanetto et al. 2006; McQuinn et al. 2007; Mesinger & Furlanetto 2008b). Clustering is a much more difficult measurement than the number density, requiring a large number of sources. It is not yet possible with the Lyman-α line sources at $z \sim 7$, but at $z \sim 6.6$ there is no evidence for an anomalous increase in clustering (McQuinn et al. 2007; Ouchi et al. 2010), indicating $Q_{\rm HII} \gtrsim 0.5$ at that time. We show this constraint with the filled diamond in Figure 5.

6.7. *Comparison to Our Models*

Figure 5 also shows the reionization history in our preferred model, with the associated confidence intervals, that extrapolates the observed luminosity function to $M_{\rm UV} = -13$. Amazingly, this straightforward model obeys all the constraints we have listed in this section, with the exception of the Fan et al. (2006b) Lyman-α forest measurements. However, we remind the reader that our crude reionization model fails at very small neutral fractions because it does not properly account for the high gas clumping in dense systems near galaxies, so we do not regard this apparent disagreement as worrisome to any degree.

It is worth considering the behavior of this model in some detail. A brief examination of the data points reveals that the most interesting limits come from the Lyman-α lines inside of galaxies (the filled pentagon, from spectroscopic followup of Lyman-break galaxies, and the open pentagons, from direct narrowband abundance at $z \sim 6.6$ and 7). These require relatively high neutral fractions at $z \sim 7$ in order for the IGM to affect the observed abundance significantly; the model shown here just barely satisfies the constraints. In a model in which we integrate the luminosity function to fainter magnitudes (e.g., $M_{\rm UV} < -10$, dotted line), the ionized fraction is somewhat higher at this time and may prevent the lines from being significantly extinguished, while a model with the minimum luminosity closer to the observed limit (e.g., $M_{\rm UV} < -17$, dashed line) reionizes the universe so late that the emitter population at $z \sim 6.6$ should have been measurably reduced.

Clearly, improvements in the measured abundance of strong line emitters at this epoch (perhaps with new multi-object infrared spectrographs, like LUCI on LBT or MOSFIRE on Keck, or with new widefield survey cameras, like HyperSuprimeCam) will be very important for distinguishing viable reionization histories. Equally important will be improvements in the modeling of the decline in the Lyman-α line emitters, as a number of factors both outside (the morphology of reionization, resonant absorption near the source galaxies, and absorption from dense IGM structures) and inside galaxies (dust absorption, emission geometry, and winds) all affect the detailed interpretation of the raw measurements (e.g., Santos 2004; Dijkstra et al. 2011; Bolton & Haehnelt 2012).

In order to have a relatively high neutral fraction at $z \sim 7$, a plausible reionization history *cannot* complete the process by $z \sim 6.4$ (to which the most distant Lyman-α forest spectrum currently extends), unless either: (1) the Lyman-continuum luminosity of galaxies, per unit 1500 $\AA$ luminosity, evolves rapidly over that interval, (2) the escape fraction $f_{\rm esc}$ increases rapidly toward lower redshifts, or (3) the abundance of galaxies below $M_{\rm UV} \sim -17$ evolves rapidly. Otherwise, the UDF12 luminosity functions have sufficient precision to fix the shape of the $Q_{\rm HII}(z)$ curve over this interval (indeed, to $z \sim 8$), and as shown in Figure 5, the slope is relatively shallow. Indeed, in our best-fit model the universe still has $1.0 - Q_{\rm HII} \sim 0.1$ at $z \sim 6$. This suggests intensifying searches for the last neutral regions in the IGM at this (relatively) accessible epoch.

Although reionization ends rather late in this best-fit model, it still satisfies the WMAP optical depth constraint (at $1-\sigma$) thanks to a long tail of low-level star formation out to very high redshifts, as suggested by Ellis et al. (2013), although the agreement is much easier if the WMAP value turns out to be somewhat high. This implies that the kinetic Sunyaev-Zel'dovich signal should have a reasonably large amount of power. Formally, our best-fit model has $\Delta z \sim 5$, according to the definition of Zahn et al. (2012), which is within the range that can be constrained if the thermal Sunyaev-Zel'dovich contamination can be sorted out. We also note that the *WMAP* results (Hinshaw et al. 2012) indicate that when combining the broadest array of available data sets, the best fit electron scattering optical depth lowers by $\sim 5\%$ to $\tau \approx 0.08$.

In summary, we have shown that the UDF12 measurements allow a model of star formation during the cosmic dawn that satisfies all available constraints on the galaxy populations and IGM ionization history, with reasonable extrapolation to fainter systems and *no assumptions about high-redshift evolution in the parameters of star formation or UV photon production and escape*. Of course, this is not to say such evolution cannot occur (see Kuhlen & Faucher-Giguère 2012, Alvarez et al. 2012, and our Section 6.2 for examples in which it does), but it does not appear to be essential.

7. SUMMARY

The 2012 Hubble Ultra Deep Field (UDF12) campaign, a 128-orbit *Hubble Space Telescope* (*HST*) program (GO 12498, PI: R. Ellis, as described in Ellis et al. 2013 and Koekemoer et al. 2013), has acquired the deepest infrared WFC3/IR images ever taken with *HST*. These observations have enabled the first identification of galaxies at $8.5 \leq z \leq 12$ in the Ultra Deep Field (Ellis et al. 2013), newly accurate luminosity function determinations at redshifts $z \sim 7-8$ (Schenker et al. 2012a; McLure et al. 2012), robust determinations of the ultraviolet spectral slopes of galaxies at $z \sim 7-8$ (Dunlop et al. 2012b), and the first estimates of the luminosity function and spectral slopes at $z \sim 9$ (McLure et al. 2012; Dunlop et al. 2012b). Synthesizing these constraints on high-redshift galaxy populations with the recent 9-year *Wilkinson Microwave Anisotropy Probe* (*WMAP*) constraints on the electron scattering optical depth generated by ionized cosmic hydrogen (Hinshaw et al. 2012) and previous determinations of the galaxy luminosity function at redshifts $4 \lesssim z \lesssim 6$

(Bouwens et al. 2007), we infer constraints on the reionization history of the universe.

First, we use the UV spectral slope $\beta = -2$ of high-redshift galaxies measured by Dunlop et al. (2012b) to constrain the available Bruzual & Charlot (2003) stellar population models consistent with the spectral character of galaxies at $z \sim 7-9$. These models motivate the adoption of a Lyman continuum photon production rate per unit UV luminosity spectral density $\log \xi_{\rm ion} = 25.2$ log ergs^{-1} Hz; the data does not favor a luminosity-dependent variation in the efficiency of Lyman continuum photon production. With this value of $\xi_{\rm ion}$ for high-redshift galaxies, and under reasonable assumptions for the Lyman continuum photon escape fraction from galaxies and the clumping factor of intergalactic gas (as motivated by cosmological simulations), we find that the currently observed galaxy population accessible to the limiting depth of UDF12 ($M_{\rm UV} < -17$ to $z \sim 8$) cannot simultaneously reionize the universe by $z \sim 6$ and reproduce the Thomson optical depth τ unless the abundance of star-forming galaxies or the ionizing photon escape fraction *increases* beyond redshift $z \sim 12$ from what is currently observed.

If we utilize constraints on the evolving galaxy luminosity function at redshifts $4 \lesssim z \lesssim 9$ to extrapolate down in luminosity, we find that the tension between the declining abundance of star-forming galaxies and their stellar mass density with redshift, the observed requirement to reionize the universe by $z \sim 6$, and reproducing the large electron scattering optical depth $\tau \approx 0.084$ is largely relieved if the galaxy population continues down to $M_{\rm UV} < -13$ and the epoch of galaxy formation continues to $z \sim 12-15$. Given the first identification of a $z \sim 12$ candidate galaxy by the UDF12 program, the prospect for high-redshift galaxies to reionize the universe is positive provided that the epoch of galaxy formation extends to $z \gtrsim 12$. Further observations by *HST* (e.g., the "Frontier Fields") and, ultimately, the *James Webb Space Telescope* will be required to answer these questions more definitively.

We thank Gary Hinshaw and David Larson for pointing us to the MCMC chains used in inferring the WMAP 9-year cosmological constraints. BER is supported by Steward Observatory and the University of Arizona College of Science. SRF is partially supported by the David and Lucile Packard Foundation. US authors acknowledge financial support from the Space Telescope Science Institute under award HST-GO-12498.01-A. RJM acknowledges the support of the European Research Council via the award of a Consolidator Grant, and the support of the Leverhulme Trust via the award of a Philip Leverhulme research prize. JSD and RAAB acknowledge the support of the European Research Council via the award of an Advanced Grant to JSD. JSD also acknowledges the support of the Royal Society via a Wolfson Research Merit award. ABR and EFCL acknowledge the support of the UK Science & Technology Facilities Council. SC acknowledges the support of the European Commission through the Marie Curie Initial Training Network ELIXIR. This work is based in part on observations made with the NASA/ESA Hubble Space Telescope, which is operated by the Association of Universities for Research in Astronomy, Inc, under NASA contract NAS5-26555.

REFERENCES

Alvarez, M. A., Finlator, K., & Trenti, M. 2012, ApJ, 759, L38
Barkana, R., & Loeb, A. 2001, Phys. Rep., 349, 125
Bolton, J. S., & Becker, G. D. 2009, MNRAS, 398, L26
Bolton, J. S., & Haehnelt, M. G. 2007a, MNRAS, 381, L35
—. 2007b, MNRAS, 382, 325
—. 2012, MNRAS, 412
Bolton, J. S., Haehnelt, M. G., Warren, S. J., Hewett, P. C., Mortlock, D. J., Venemans, B. P., McMahon, R. G., & Simpson, C. 2011, MNRAS, 416, L70
Bouwens, R. J., Illingworth, G. D., Franx, M., & Ford, H. 2007, ApJ, 670, 928
Bouwens, R. J., et al. 2012a, ApJ, 754, 83
—. 2012b, ApJ, 752, L5
—. 2010, ApJ, 708, L69
Bruzual, G., & Charlot, S. 2003, MNRAS, 344, 1000
Carilli, C. L., et al. 2010, ApJ, 714, 834
Cen, R. 2003, ApJ, 591, 12
Chabrier, G. 2003, PASP, 115, 763
Charlot, S., & Fall, S. M. 2000, ApJ, 539, 718
Chen, H.-W., Prochaska, J. X., & Gnedin, N. Y. 2007, ApJ, 667, L125
Choudhury, T. R., Haehnelt, M. G., & Regan, J. 2009, MNRAS, 394, 960
Ciardi, B., Bolton, J. S., Maselli, A., & Graziani, L. 2012, MNRAS, 423, 558
Ciardi, B., Ferrara, A., & White, S. D. M. 2003, MNRAS, 344, L7
Dayal, P., & Ferrara, A. 2012, MNRAS, 421, 2568
Dijkstra, M., Mesinger, A., & Wyithe, J. S. B. 2011, MNRAS, 414, 2139
Djorgovski, S. G., Castro, S., Stern, D., & Mahabal, A. A. 2001, ApJ, 560, L5
Dunkley, J., et al. 2011, ApJ, 739, 52
Dunlop, J. S., McLure, R. J., Robertson, B. E., Ellis, R. S., Stark, D. P., Cirasuolo, M., & de Ravel, L. 2012a, MNRAS, 420, 901
Dunlop, J. S., et al. 2012b, arXiv:1212.0860
Ellis, R. S., et al. 2013, ApJ, 763, L7
Fan, X., Carilli, C. L., & Keating, B. 2006a, ARA&A, 44, 415
Fan, X., et al. 2001, AJ, 122, 2833
Fan, X., Narayanan, V. K., Strauss, M. A., White, R. L., Becker, R. H., Pentericci, L., & Rix, H.-W. 2002, AJ, 123, 1247
Fan, X., et al. 2006b, AJ, 132, 117
—. 2003, AJ, 125, 1649
Faucher-Giguère, C.-A., Lidz, A., Hernquist, L., & Zaldarriaga, M. 2008, ApJ, 688, 85
Faucher-Giguère, C.-A., Lidz, A., Zaldarriaga, M., & Hernquist, L. 2009, ApJ, 703, 1416
Feroz, F., & Hobson, M. P. 2008, MNRAS, 384, 449
Feroz, F., Hobson, M. P., & Bridges, M. 2009, MNRAS, 398, 1601
Ferrara, A., & Loeb, A. 2012, ArXiv e-prints
Finkelstein, S. L., Papovich, C., Giavalisco, M., Reddy, N. A., Ferguson, H. C., Koekemoer, A. M., & Dickinson, M. 2010, ApJ, 719, 1250
Finkelstein, S. L., et al. 2012, ApJ, 756, 164
Finlator, K., Oh, S. P., Özel, F., & Davé, R. 2012, MNRAS, 427, 2464
Fontana, A., et al. 2010, ApJ, 725, L205
Fontanot, F., Cristiani, S., & Vanzella, E. 2012, MNRAS, 425, 1413
Furlanetto, S. R., Hernquist, L., & Zaldarriaga, M. 2004a, MNRAS, 354, 695
Furlanetto, S. R., & Oh, S. P. 2005, MNRAS, 363, 1031
—. 2009, ApJ, 701, 94
Furlanetto, S. R., Zaldarriaga, M., & Hernquist, L. 2004b, ApJ, 613, 1
—. 2006, MNRAS, 365, 1012
Gnedin, N. Y. 2000, ApJ, 535, 530
Gnedin, N. Y., & Ostriker, J. P. 1997, ApJ, 486, 581
González, V., Labbé, I., Bouwens, R. J., Illingworth, G., Franx, M., & Kriek, M. 2011, ApJ, 735, L34
Gruzinov, A., & Hu, W. 1998, ApJ, 508, 435
Gunn, J. E., & Peterson, B. A. 1965, ApJ, 142, 1633
Haardt, F., & Madau, P. 2012, ApJ, 746, 125
Hinshaw, G., et al. 2012, arXiv:1212.5226
Hou, Z., Keisler, R., Knox, L., Millea, M., & Reichardt, C. 2011, arXiv:1104.2333
Hu, E. M., Cowie, L. L., McMahon, R. G., Capak, P., Iwamuro, F., Kneib, J.-P., Maihara, T., & Motohara, K. 2002, ApJ, 568, L75
Hui, L., & Haiman, Z. 2003, ApJ, 596, 9
Iliev, I. T., Mellema, G., Pen, U.-L., Merz, H., Shapiro, P. R., & Alvarez, M. A. 2006, MNRAS, 369, 1625

Jensen, H., Laursen, P., Mellema, G., Iliev, I. T., Sommer-Larsen, J., & Shapiro, P. R. 2013, MNRAS, 428, 1366
Jones, T., Stark, D. P., & Ellis, R. S. 2012, ApJ, 751, 51
Kashikawa, N., et al. 2006, ApJ, 648, 7
Knox, L., Scoccimarro, R., & Dodelson, S. 1998, Physical Review Letters, 81, 2004
Koekemoer, A. M., et al. 2013, ApJS, submitted, arXiv:1212.1448
Kuhlen, M., & Faucher-Giguère, C.-A. 2012, MNRAS, 423, 862
Labbe, I., et al. 2012, arXiv:1209.3037
Lidz, A., Oh, S. P., & Furlanetto, S. R. 2006, ApJ, 639, L47
Loeb, A., & Furlanetto, S. 2012, The First Galaxies in the Universe (Princeton University Press)
Madau, P., Haardt, F., & Rees, M. J. 1999, ApJ, 514, 648
Madau, P., Pozzetti, L., & Dickinson, M. 1998, ApJ, 498, 106
Malhotra, S., & Rhoads, J. E. 2004, ApJ, 617, L5
McGreer, I. D., Mesinger, A., & Fan, X. 2011, MNRAS, 415, 3237
McLure, R. J., et al. 2012, arXiv:1212.5222
—. 2011, MNRAS, 418, 2074
McQuinn, M., Hernquist, L., Zaldarriaga, M., & Dutta, S. 2007, MNRAS, 381, 75
McQuinn, M., Lidz, A., Zaldarriaga, M., Hernquist, L., & Dutta, S. 2008, MNRAS, 388, 1101
McQuinn, M., Oh, S. P., & Faucher-Giguère, C.-A. 2011, ApJ, 743, 82
Mesinger, A. 2010, MNRAS, 407, 1328
Mesinger, A., & Furlanetto, S. R. 2008a, MNRAS, 385, 1348
—. 2008b, MNRAS, 386, 1990
Mesinger, A., & Haiman, Z. 2004, ApJ, 611, L69
Mesinger, A., McQuinn, M., & Spergel, D. N. 2012, MNRAS, 422, 1403
Meurer, G. R., Heckman, T. M., & Calzetti, D. 1999, ApJ, 521, 64
Miralda-Escudé, J. 1998, ApJ, 501, 15
Miralda-Escudé, J., Haehnelt, M., & Rees, M. J. 2000, ApJ, 530, 1
Miralda-Escudé, J., Haehnelt, M., & Rees, M. J. 2000, ApJ, 530, 1
Mitra, S., Ferrara, A., & Choudhury, T. R. 2013, MNRAS, 428, L1
Mortlock, D. J., et al. 2011, Nature, 474, 616
Muñoz, J. A., & Loeb, A. 2011, ApJ, 729, 99
Muñoz, J. A., Trac, H., & Loeb, A. 2010, MNRAS, 405, 2001
Oesch, P. A., et al. 2009, ApJ, 690, 1350
Oke, J. B., & Gunn, J. E. 1983, ApJ, 266, 713
Ono, Y., et al. 2012a, arXiv:1212.3869
—. 2012b, ApJ, 744, 83
Ono, Y., Ouchi, M., Shimasaku, K., Dunlop, J., Farrah, D., McLure, R., & Okamura, S. 2010, ApJ, 724, 1524
Ostriker, J. P., & Vishniac, E. T. 1986, ApJ, 306, L51
Ota, K., et al. 2008, ApJ, 677, 12
Ouchi, M., et al. 2009, ApJ, 706, 1136
—. 2010, ApJ, 723, 869
Pawlik, A. H., Schaye, J., & van Scherpenzeel, E. 2009, MNRAS, 394, 1812
Pentericci, L., et al. 2011, ApJ, 743, 132
Prochaska, J. X., Worseck, G., & O'Meara, J. M. 2009, ApJ, 705, L113
Razoumov, A. O., Norman, M. L., Abel, T., & Scott, D. 2002, ApJ, 572, 695
Reichardt, C. L., et al. 2012, ApJ, 755, 70
Robertson, B., Li, Y., Cox, T. J., Hernquist, L., & Hopkins, P. F. 2007, ApJ, 667, 60
Robertson, B. E. 2010a, ApJ, 716, L229
—. 2010b, ApJ, 713, 1266
Robertson, B. E., Ellis, R. S., Dunlop, J. S., McLure, R. J., & Stark, D. P. 2010, Nature, 468, 49
Rogers, A. B., McLure, R. J., & Dunlop, J. S. 2012, arXiv:1209.4636
Salpeter, E. E. 1955, ApJ, 121, 161
Salvaterra, R., Ferrara, A., & Dayal, P. 2011, MNRAS, 414, 847
Santos, M. R. 2004, MNRAS, 349, 1137
Santos, M. R., & others. 2004, ApJ, 606, 683
Schaerer, D. 2003, A&A, 397, 527
Schaerer, D., & de Barros, S. 2009, A&A, 502, 423
—. 2010, A&A, 515, A73
Schechter, P. 1976, ApJ, 203, 297
Schenker, M. A., et al. 2012a, arXiv:1212.4819
Schenker, M. A., Stark, D. P., Ellis, R. S., Robertson, B. E., Dunlop, J. S., McLure, R. J., Kneib, J.-P., & Richard, J. 2012b, ApJ, 744, 179
Schroeder, J., Mesinger, A., & Haiman, Z. 2012, arXiv:1204.2838
Shull, J. M., Harness, A., Trenti, M., & Smith, B. D. 2012, ApJ, 747, 100
Simcoe, R. A., Sullivan, P. W., Cooksey, K. L., Kao, M. M., Matejek, M. S., & Burgasser, A. J. 2012, Nature, 492, 79
Sokasian, A., Abel, T., Hernquist, L., & Springel, V. 2003, MNRAS, 344, 607
Songaila, A., & Cowie, L. L. 2010, ApJ, 721, 1448
Spergel, D. N., et al. 2003, ApJS, 148, 175
Stark, D. P., Ellis, R. S., Chiu, K., Ouchi, M., & Bunker, A. 2010, MNRAS, 408, 1628
Stark, D. P., Schenker, M. A., Ellis, R. S., Robertson, B., McLure, R., & Dunlop, J. 2012, arXiv:1208.3529
Totani, T., Kawai, N., Kosugi, G., Aoki, K., Yamada, T., Iye, M., Ohta, K., & Hattori, T. 2006, PASJ, 58, 485
Trac, H., Cen, R., & Loeb, A. 2008, ApJ, 689, L81
Treu, T., Trenti, M., Stiavelli, M., Auger, M. W., & Bradley, L. D. 2012, ApJ, 747, 27
Willott, C. J., et al. 2010, AJ, 139, 906
Wyithe, J. S. B., & Loeb, A. 2003, ApJ, 586, 693
Zahn, O., et al. 2012, ApJ, 756, 65